We are very grateful to the two reviewers for their valuable comments and suggestions. A summary of the main changes in the revised manuscript is as follows:

1 In the "Introduction" section, information about the study area (lakes, glaciers) is updated using the new numbers from the recent literature. The hypothesis that the subsidence volume equals to ground ice melting supply is elaborated.

2 In the "3.3.1 SBAS-InSAR processing" section, some statements are refined, and methods of evaluating the quality of unwrapped phases and inverted raw phase time series are added.

3 In the "4.1 Lake water storage changes", the tracks of the ICESat-2 elevation measurements for each year are added in Figure 4, and the calculation of lake water storage change was elaborated.

4 In the "4.2 Ground surface deformation" section, the deformation values were updated after reprocessing of deformation time series estimation.

5 In the "4.4.1 Uncertainties and accuracies of lake volume changes" section, lake area and volume changes were reviewed from the literature and compared with the values during the study period.

6 In the "4.4.2 Uncertainties and accuracies of deformation" section, the quality of unwrapped phases and inverted raw phase time series were evaluated.

7 In the "5.1 Uplift displacement signal" section, the deformation maps are displayed with optical images and topography maps, and the discussion of the uplift signal has been adjusted and

8 Figures have been replotted for better readability. Figures of the interferogram network, deformation maps from orbits 48 and 150, and enlarged deformation maps of the field investigation region are added in the Appendix.

Below are our itemized replies to these comments. The comments from the reviewer are shown in blue, with the responses shown in black.

Response to Reviewer #1

In this study, Wang et al. estimated deformation rate of permafrost in the Selin Co basin by Sentinel-1 SAR data. The subsidence volume was assumed as ground ice melting. The contribution (ratio) of ground ice melting to lake water volume gain was estimated. This study first quantified the contribution of ground ice change to the expansion of Serlin Co. This study is novel and suitable to publish in Cryosphere after further improvement/clarification.

The authors are very grateful for the valuable comments and suggestions from the reviewer.

Detailed responses and revisions based on the comments are listed below.

Major comments:

1) In this study, the contribution of ground ice melting to water volume increase of Selin Co was estimated by subsidence space derived from Sentinel-1 SAR data. The ice density of 0.91 g/cm3 was used to estimated the water released from ground ice into lake. This process is not easy to understand. The authors can add more interoperation of this hypothesis that the subsidence volume equals to ground ice melting supply is reasonable.

Thank you very much for the comment. We have added more interoperation of this hypothesis in the "Introduction" and "Method" sections.

In the "Introduction" section, we first stated that "Significant permafrost degradation has been observed on the TP under the impacts of the warming climate. The monitoring of ten boreholes on the TP revealed that from 1981 to 2018, the active layer thickened at an average rate of 19.5 cm per decade; moreover, this thickening trend has been accelerating in recent years (Zhao et al., 2020). In the meantime, different permafrost regions across the TP experienced thaw settlements (Daout et al., 2017; Chen et al., 2022). The ice content within the uppermost layer of permafrost is typically higher than the saturated water content after this permafrost layer thaws; hence, the thawing of this layer might result in terrain settlement (Streletskiy et al., 2016; Shiklomanov et al., 2013; Günther et al., 2015; Lantuit and Pollard, 2008; Kokelj and Jorgenson, 2013). The terrain settlement was attributed to the melting of ground ice from the ice-rich permafrost layer just below the permafrost table and the further release of this water into the hydrological cycle (Zhao et al., 2019)", then stated "It is well known that the permafrost layer just below the permafrost table always contains ground ice higher than 50% in volume (Cheng, 1983; Mackay, 1983; French and Harbor, 2013; Zhao and Sheng, 2019). Therefore, we assumed that the amount of surface settlement would release the same amount of ground ice caused by compressing the thawing ice-rich permafrost layer.".

In the Method section "3.4 Conversion from ground deformation to ground ice meltwater contribution", we stated that "A considerable amount of ground ice is always buried in permafrost regions, especially just below the permafrost table (Cheng, 1983; Mackay, 1983; French and Harbor, 2013). Thawing of the uppermost permafrost layer is always accompanied by the compaction of sediment and subsidence of the ground surface due to the melting of super-saturated ground ice (French, 2017). Hence, the higher the ice content in permafrost, the larger the surface subsidence occurred as it was thawed. In this study, we assume that the long-term cumulated settlement is equal to the thickness of ground ice melted, and then released to the hydrological cycle.".

2) This study only presents three-year study from 2017 to 2020. How the lake volume and space of subsidence were estimated and uncertainties? ICESat-2 stared from 2018, how about the data in 2017? The authors could include a comparison (lake level/volume changes) in discussion with a supplementary table with previous studies?

Thank you very much for the comment and suggestion.

1) To be clear, **we have added the statements in the revised manuscript as "To calculate the changes in the** lake water storage of Selin Co, Eq. (1) was applied taking the areas of 2408.1 km^2 in 2018 and 2441.2 km^2 in 2020 and taking the water surface elevation change of ~0.4 m between these two years; then, the change in lake volume from 2018 to 2020 was estimated, and finally, the annual volume change rate was obtained by dividing the results of these two years. The annual rate of change in the lake volume of Selin Co during 2018–2020 was ~485×10^6 m^3/a." Both the subsidence and lake volume change are expressed in the way of rates. Although there is a slight inconsistency between their periods, they could represent the characteristics of this certain period.

2) Taking the reviewer's suggestion, **we have reviewed the changes in the lake area, water level, and water volume in previous studies and compared them with our results.** Lake area change information are from (Zhu et

al., 2019b; Qiao et al., 2019; Meng et al., 2012; Sun et al., 2020; Zhang et al., 2020; Deij et al., 2018); water level change information are from (Meng et al., 2012; Lei et al., 2013; Doin et al., 2015; Zhang et al., 2013; Sun et al., 2020; Hwang et al., 2019; Zhang et al., 2020; Zhu et al., 2019a); and water volume information are from (Zhu et al., 2019b; Qiao et al., 2019; Treichler et al., 2019; Sun et al., 2020; Zhang et al., 2013; Li et al., 2019).The changes in lake area, lake level, and volume are shown in Fig. 10 in the revised manuscript.

Figure 10 Comparisons of the changes in the lake area (subfigure a) water surface elevation (b) and lake volume (c) of Selin Co with historical values.

We have stated in the discussion section "4.4.1 Uncertainties and accuracies of lake volume change rate" that "Our analysis shows that during the period of 2018–2020, the water level increased at a rate of ~0.2 m/a, the lake area increased at a rate of 10.3 km^2/a, and the lake water storage increased at a rate of 485×10^6 m^3/a. These values are compared with those recorded in previous studies in Fig. 10. lake area change information are from (Zhu et al., 2019b; Qiao et al., 2019; Meng et al., 2012; Sun et al., 2020; Zhang et al., 2020; Deij et al., 2018); water level change information are from (Meng et al., 2012; Lei et al., 2013; Doin et al., 2015; Zhang et al., 2013; Sun et al., 2020; Hwang et al., 2019; Zhang et al., 2020; Zhu et al., 2019a); and water volume information are from (Zhu et al., 2019b; Qiao et al., 2019; Treichler et al., 2019; Sun et al., 2020; Zhang et al., 2013; Li et al., 2019). As illustrated in Fig. 10, the expansion of Selin Co was slow before 2000, with lake area and volume increases of 9.1 km^2/a and 368×10^6 m^3/a, respectively. Then, in the period of 2000–2005, the lake expanded extremely fast, with the water level increasing at an approximate rate of 1.0 m/a and the lake area and volume increasing at rates of 60.7 km^2/a and 1576×10^6 m^3/a, respectively. After 2005, however, these rates of increase slowed down, with

those of the lake area and lake water storage slowing to only 12.6 km^2/a and 553×10^6 m^3/a during 2005–2017, respectively, and the rate of increase in the water surface elevation slowing to 0.2 m/a during 2007–2011 (Doin et al., 2015). Overall, the values retrieved in this study are all within the ranges of the historical values and are closest to the values after the 2010s."

3) Regarding the uncertainties of spatial deformation, we used two indicators that qualitatively evaluated the quality of unwrapped phases and inverted raw phase time series: the phase closure of interferogram triplets and temporal coherence. Their meanings are described in section 3.3.1 SBAS-InSAR processing ii) Deformation time series estimation as follows.

Two indicators evaluated the quality of unwrapped phases and inverted raw phase time series: the phase closure of interferogram triplets and temporal coherence. The phase unwrapping algorithms add integer number of 2π phase jumps to recover the unwrapped phase. Interferometric phase noise and discontinuities among different coherent regions may lead to the wrong 2π jumps added to the phase field known as unwrapping error. Unwrapping errors can bias the estimated time series. For an interferogram triplet ($\Delta\phi^{ij}$, $\Delta\phi^{jk}$ and $\Delta\phi^{ik}$), unwrapping errors introduce a nonzero integer component C_{int}^{ijk} in the closure phase C^{ijk}. Therefore, the number of interferogram triplets with nonzero integer ambiguity T_{int} can be used to detect unwrapping errors:

$$C^{ijk} = \Delta\varphi^{ij} + \Delta\varphi^{jk} - \Delta\varphi^{ik} \tag{2}$$

$$C_{int}^{ijk} = \frac{C^{ijk} - \text{wrap}\,(C^{ijk})}{2\pi} \tag{3}$$

$$T_{int} = \sum_{i=1}^{T} \left(C_{int}^{ijk}! = 0 \right) \tag{4}$$

where $\Delta\varphi^{ij}$, $\Delta\varphi^{jk}$ and $\Delta\varphi^{ik}$ are the three unwrapped interferometric phases generated from the SAR acquisitions at t_i, t_j and t_k, respectively; wrap is an operator that wraps each input number into $[-\pi, \pi)$; and T is the number of interferogram triplets. A triplet without unwrapping errors has $C_{int}^{ijk} \equiv 0$.

The second index, temporal coherence, represents the consistency of the time series with the network of interferograms (Pepe and Lanari, 2006):

$$\gamma_{temp} = \frac{1}{M}\left|H^T \exp\left[j(\Delta\phi - A\widehat{\phi})\right]\right| \tag{5}$$

where (for N SAR images and M interferograms) $\Delta\phi$ is the unwrapped interferometric phase; A is the $M \times (N - 1)$ design matrix indicating the acquisition pairs used for interferograms generation (consisting of -1, 0 and 1 for each row with -1 for the reference acquisition, 1 for the secondary acquisition and 0 for all other acquisitions (Berardino et al., 2002)); $\widehat{\phi}$ denotes the estimated time series; H is an M×1 all-ones column vector; and j is the imaginary unit.

Temporal coherence varies from 0 to 1: pixels with values closer to 1 are considered reliable, whereas pixels with values closer to zero are considered unreliable.

The uncertainties and accuracy of deformation time series estimation are stated in section 4.4.2 Uncertainties and accuracies of deformation, as follows.

Fig. 11 shows the spatial distribution of the number of interferogram triplets with nonzero integer ambiguity T_{int} (Eq(4) in the manuscript), with the histogram illustrating the distribution of T_{int} values within the Selin Co watershed excluding glaciers and water bodies. The areas having T_{int} smaller than three take part 95% of the

watershed, while 72.3% of the watershed has T_{int} value of zero (no wrapping error on all the interferograms). The value of T_{int} evaluated the quality of original interferometric unwrapped phases, the unwrapping errors could be further reduced by bridging reliable regions before network revision (Zhang et al., 2019).
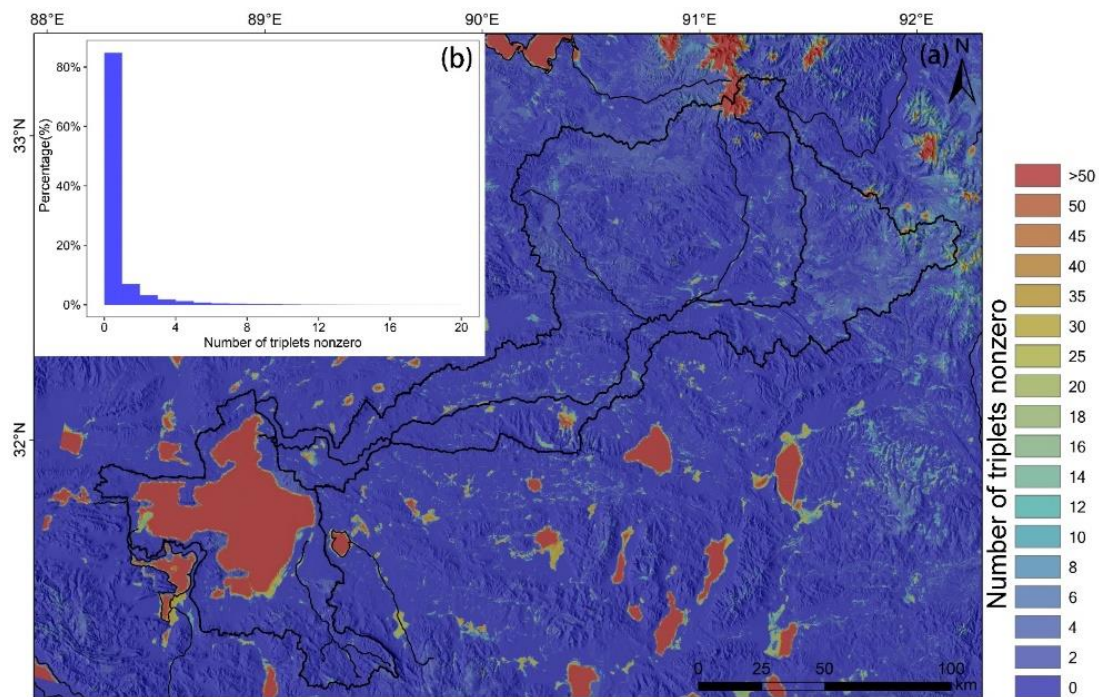
Figure 11 (a) Map of the number of interferogram triplets with nonzero integer ambiguity T_{int} (Eq(4)), (b) histogram illustrating the distribution of T_{int} values within the Selin Co watershed excluding glaciers and water bodies.

Fig. 12 shows the spatial distribution of temporal coherence (Eq.(5) in the manuscript), which is used to evaluate the quality of raw phase time series. 99.0% of the watershed has temporal coherence higher than 0.8, 98.1% has temporal coherence higher than 0.85, 96.0% has temporal coherence higher than 0.9 and 89.1% has temporal coherence higher than 0.95.
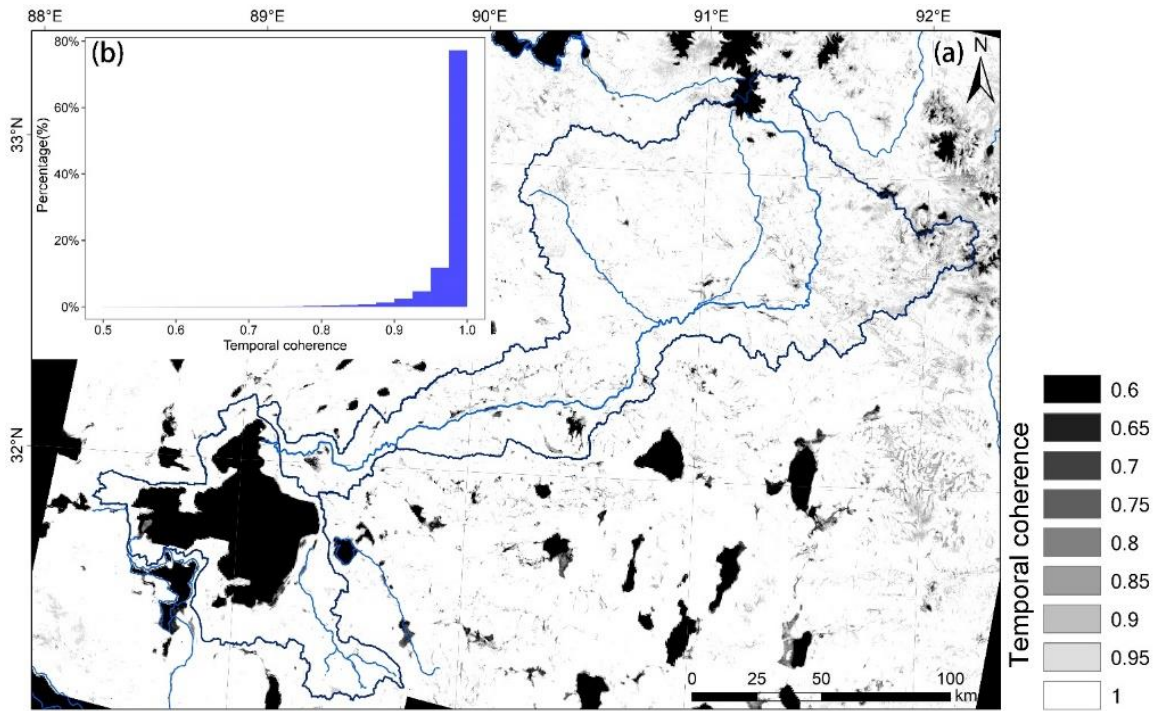
Figure 12 (a) Map of temporal coherence (Eq(5)), (b) histogram illustrating the distribution of temporal coherence values within the Selin Co watershed excluding glaciers and water bodies.

3) The uncertainties (plus minus) of all estimates could be included.

Thank you. In the previous manuscript, the ground ice meltwater volume was calculated considering two extreme situations regarding the uplift signal. But due to a lack of field investigation, it is hard to attribute the uplift signal absolutely to permafrost aggradation or the rise of the groundwater table or sedimentation. Thus, we only presented the uplift signal and discussed this phenomenon in the discussion section. The volume value caused by the uplift signal is small compared to that calculated by subsidence. Thus, the revised manuscript no longer provides the estimated volume considering two extreme situations.

4) Figure 4: The seasonal cycle of lake level looks strange. Please check your data and compare with other studies.

Thank you for the comment. The lake level data has been checked and examined. In the previous manuscript, the mask used to extract the ICESat-2 measurements located in the lake is the lake extent of 2020. To avoid some unstable values in the lake shores of the year 2018 and 2019, in the revised manuscript, we used the water mask of the corresponding year. The tracks of ICESat-2 in each year were presented in Fig. 4(a)-(c) as follows.
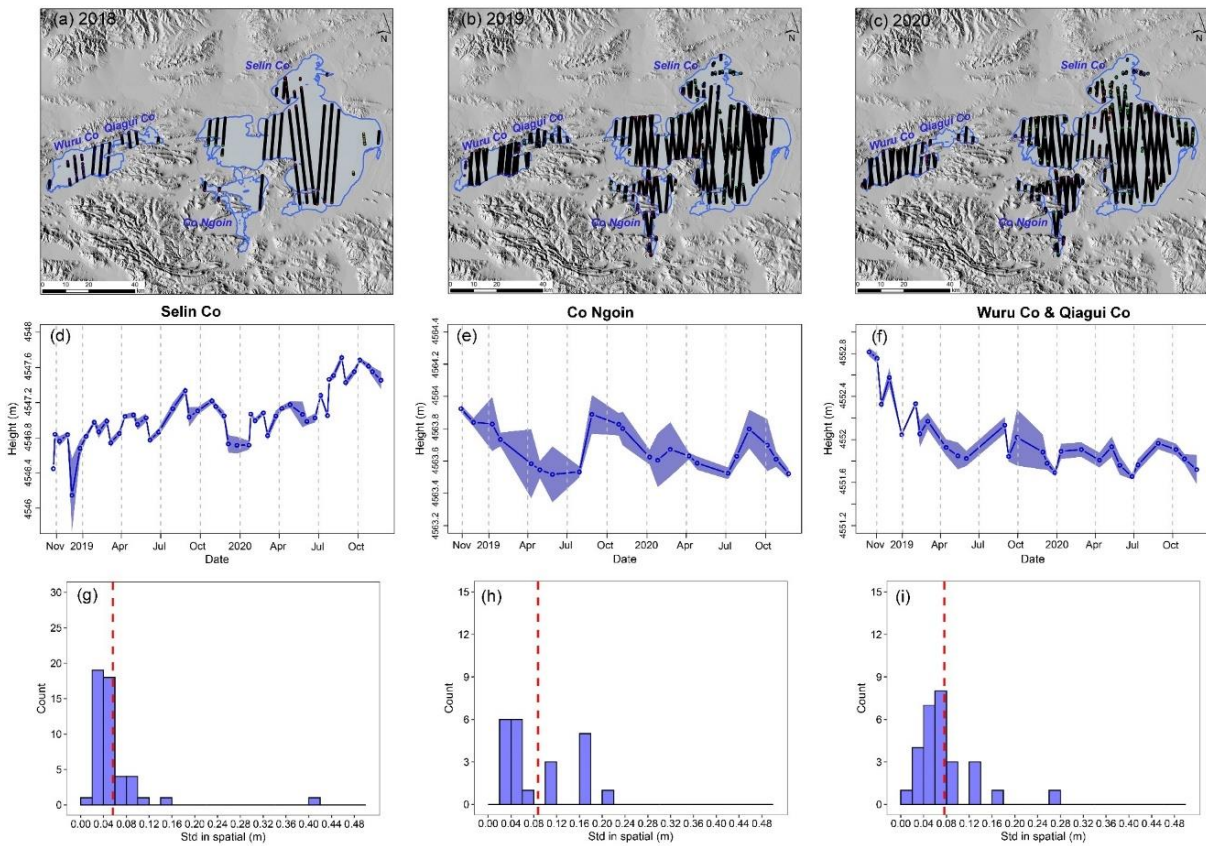
Figure 4 Water surface elevations of the three lakes. Subfigures (a)-(c) show tracks of the elevation measurements for each year. Sufigures (d)-(f) show the ICESat-2 derived elevations. The solid lines indicate the average values of all elevation measurements within the lake on a given date. The light-colored areas show the mean ± one standard deviation. Subfigures (g)-(i) further show histograms of the standard deviations of the water surface elevation of the lake from all acquisition dates. The Red dashed line indicates the mean value.

The Co Ngoin shows a clear periodic seasonal cycle in which the lake level was low during April-July and high during September-November. Wuru Co & Qiqgui Co also illustrate that the water level is higher in September-October than in the other months. The possible explanation might be the strong evaporation during April-August reduced water level. Although the water level of Selin Co fluctuates a lot, it also manifests some trend that the water level increases from July to October. It also reveals the pattern stated in other studies that the Selin Co's water level reaches a stable maximum during October and November.

5) Table 6: How the surface water elevation for each year was decided? The mean or level in a month was used/selected? The column of velocity is no value and can be removed.

Thank you for the comment. To be clear, we have stated in the revised manuscript that the surface water elevation listed in Table 6 was the averaged value of all elevation measurements of the lake within each year. In the revised manuscript, the mean ± one standard deviation of all elevation measurements of the lake within the year were listed in Table 6. The tracks of ICESat-2 elevation measurements are shown

6) The English writing of this manuscript need improve. It is better to polish by a native English speaker. For example, Line 375, too many "them had amplitudes" was used.

Thank you for the suggestion. The language has been polished.

- Serling Co lake to Serlin Co throughout, not include lake as Co means lake in Tibetan.

Thank you. We have modified it throughout the manuscript.

- "increases in precipitation and glacial melting are not enough to explain the increased water volume of lake expansion" How to understand this? The previous studies have closed the lake water balance.

To be clear, we have stated in the Abstract that "Selin Co, located within permafrost regions surrounded by glaciers, has exhibited the greatest increase in water storage among all the lakes on the Tibetan Plateau over the last 50 years. Most of the increased lake water volume has been attributed to increased precipitation and the accelerated melting of glacier ice, but these processes are still not sufficient to achieve the water balance with the expansion of Selin Co. Ground ice meltwater released by thawing permafrost due to continuous climate warming over the past several decades was regarded as another source of lake expansion."

Although the contribution of each item (precipitation, glacier meltwater, permafrost meltwater, evaporation) could be estimated from the model perspective (Zhang et al., 2017), there is still ambiguities of water balance from the monitoring perspective and the water balance is at stake.

According to the work of "Limited contribution of glacier mass loss to the recent increase in Tibetan Plateau lake volume, Brun, F., Treichler, D., Shean, D., & Immerzeel, W. W. (2020). Frontiers in Earth Science, 8, 495. DOI: 10.3389/feart.2020.582060" recommended by the reviewer, in Selin Co basin the water excess considering the changes in the lake and glacier water storage is 34.8 ± 3.4 mm/yr, and Δ (Precipitation-evapotranspiration) is 15 mm/yr.

In recent years, the contribution from the glacier has become much clear. Then the uncertainties mainly come from quantifying the contribution of increasing precipitation and thawing permafrost. The quantification of increasing precipitation contribution is still challenging. The accurate monitoring of precipitation/snow in TP is challenging work without reliable measurement.

- Line 20: the long-term, I do not suggest to use this as the short study period.

Thank you very much for the comment. The word has been replaced with "cumulated settlement" in the revised manuscript.

- Line 35: Tibetan Plateau to Tibetan Plateau (TP), and use TP thereafter.

Thank you. They have been corrected through the manuscript.

- Line 35: 1000 lakes, 40,000 km^2, please use new values.

Thank you.

Based on the newest reference of "Zhang, G., Ran, Y., Wan, W., Luo, W., Chen, W., Xu, F., & Li, X. (2021). 100 years of lake evolution over the Qinghai–Tibet Plateau. Earth System Science Data, 13(8), 3951-3966." that "The

Qinghai–Tibet Plateau has ∼ 1200 lakes larger than 1 km^2 with a total area of ∼ 46 000 km^2… The QTP includes 87 % of the lakes of the TP and 92 % of their area".

Accordingly, we have modified the statement as "More than 1200 lakes on the Tibetan Plateau (TP) span an area exceeding 1 km^2, and the total lake area is greater than 46000 km^2 (Zhang et al., 2021b)"

- Line 40: lake area and volume increase to 2017, please use the value from new published paper updated to 2019

Thank you for the suggestion. The values have been updated, and the sentence has been modified as "In particular, Selin Co (also known as Siling Co, Serlin Co, and Serling Co) exhibited the greatest increases in both lake area and water storage: its lake area expanded by ~40% from ~1700 km^2 in 1972 to ~2400 km^2 in 2020, and its water storage increased by 80% from 309.4×10^8 m^3 in 1972 to 558.4×10^8 m^3 in 2017 (Zhu et al., 2019b; Zhang et al., 2021b)."

- surpassed Nam Co lake in 2014, it is about 2011, please check new published paper, and include the citation.

Thank you for the comment. We checked the lake area of these two lakes during 2005–2013 in the lake data sets and the relevant literature (Zhang et al., 2021b; Bian et al., 2010)", and found that 2001-2005 might be the period of surpassing Nam Co. In the manuscript, the sentence has been modified as "Its lake area surpassed that of Nam Co in the early 2000s (Zhang et al., 2021b; Bian et al., 2010); consequently, Selin Co is now the second largest saltwater lake in China. Such rapid changes in Selin Co have significantly affected the regional environment and have thus attracted substantial interest within the scientific community.

- Line 45: For the statistics of glacier number and area, please use the data from the second China glacier inventory.

Thank you for the comment and suggestion.

The numbers have been calculated and updated according to the second China glacier inventory in the revised manuscript. It has been revised as "The entire Selin Co watershed covers a drainage area of 4.4×10^4 km^2, 18 times the lake surface. The entire watershed hosts 299 glaciers with a total area of 369.7 km^2 and ice reserves of 27.9 km^3 based on the second Chinese glacier inventory (Guo et al., 2015; Liu et al., 2012)"

- the ground ice volume in the watershed reaches 132.3 km^3 (Zhao and Sheng, 2019). How about the value compared with Farinotti et al. (2019) (doi: 10.1038/s41561-019-0300-3)?

Thank you very much for the literature.

Based on the dataset published in the work "Farinotti, D., Huss, M., Fürst, J. J., Landmann, J., Machguth, H., Maussion, F., & Pandit, A. (2019). A consensus estimate for the ice thickness distribution of all glaciers on Earth. Nature Geoscience, 12(3), 168-173", the Selin Co basin has 377 glaciers with a total area of 289.1 km^2 and ice volume of 21.8 km^3. Based on the second Chinese glacier inventory (Guo et al., 2015; Liu et al., 2012), the glacier ice volume is 27.9 km^3. The two numbers both indicate that the ground ice volume is about five times the glacier ice volume.

In the revised manuscript, we have included the number of glacier ice volume from Farinotti et al. (2019) and the

ratio number with ground ice. It is stated as follows "The entire Selin Co watershed covers a drainage area of 4.4×10^4 km^2, 18 times the lake surface. The entire watershed hosts 299 glaciers with a total area of 369.7 km^2 and ice reserves of 27.9 km^3 based on the second Chinese glacier inventory (Guo et al., 2015; Liu et al., 2012); additionally, according to the new estimation by (Farinotti et al., 2019), the glacier volume reaches 21.8 km^3 in the watershed……the ground ice volume in the watershed reaches 132.3 km^3 (Zhao and Sheng, 2019), approximately five times the glacier ice volume in the Selin Co watershed."

- glacial meltwater contributed ~ 10% of the total water input to Serling Co lake since the 1970s (Lei et al., 2013; Tong et al., 2016). The two other studies (doi: 10.3389/feart.2020.582060; doi: 10.1016/j.scitotenv.2021.145463) for the estimates could be included for comparison together.

Thank you very much for providing these two new studies.

Study "Zhang, G., Bolch, T., Chen, W., & Crétaux, J. F. (2021). Comprehensive estimation of lake volume changes on the Tibetan Plateau during 1976–2019 and basin-wide glacier contribution. Science of the Total Environment, 772, 145463. DOI: 10.1016/j.scitotenv.2021.145463" revealed that during 2000-2015, the glacier contribution for Selin Co is ~8.2%.

Study "Brun, F., Treichler, D., Shean, D., & Immerzeel, W. W. (2020). Limited contribution of glacier mass loss to the recent increase in Tibetan Plateau lake volume. Frontiers in Earth Science, 8, 495. DOI: 10.3389/feart.2020.582060" revealed that during the 2000s and 2010s, the glacier contribution for Selin Co is 8 ± 3%.

The two other studies have been included in the revised manuscript and the sentence has been rephrased as follows "In addition, recent research has revealed that glacial meltwater has contributed ~ 10% of the total water input to Selin Co since the 1970s (Lei et al., 2013; Tong et al., 2016; Brun et al., 2020; Zhang et al., 2021a)."

- The weakening of lake evaporation has also contributed to the accelerated expansion of Serling Co lake. It is really weaking? It should be increasing as the warmer air temperature, and some studies have corrected this by Nam Co or different study period?

The statement is based on the work "Guo, Y., Zhang, Y., Ma, N., Xu, J., & Zhang, T. (2019). Long-term changes in evaporation over Siling Co Lake on the Tibetan Plateau and its impact on recent rapid lake expansion. Atmospheric research, 216, 141-150."

This work found that "during the studying period of 1961–2015, the temporal variations in lake evaporation can be divided into three periods as follows: a significant increasing trend (12.3 mm yr-1) during the period 1961–1984, a significant decreasing trend (-10.2 mm yr-1) during the period 1985–2006, and a slightly increasing trend (4.3 mm) during the period 2007–2015. During the period of significant expansion of Siling Co Lake from 1972 to 2010, lake evaporation presented a significant decreasing trend (-4.7 mm yr-1)." The main factors that controlled the changes in evaporation were wind speed for the period 1961–2006. That explains although the air temperature is continuously increasing, the evaporations have variations.

To be clear, in the revised manuscript, we have rephrased the sentence to "The weakening of lake evaporation during 1972–2010 due to decreasing wind speeds also contributed to the accelerated expansion of Selin Co to

some extent, but this contribution was reported to be very small (Guo et al., 2019)."

- Table 2. Ele. (m) to Ele. (m a.s.l.)
Corrected.

- Line 245: ERA-5 reanalysis data, how about ERA-6 data? It is better?
ERA5 is the fifth generation ECMWF atmospheric reanalysis of the global climate. The production of the next full-observing-system reanalysis, ERA6, is planned to start by 2023 according to the newsletter of ECMWF. The accurate description of vertical profiles of temperature, pressure, and water vapor partial pressure is good for the accurate estimation and correction of tropospheric delay in InSAR phase. When good atmospheric data is not available, if SAR acquisitions are adequate and interferogram pairs have some redundancy, the tropospheric disturbances could also be removed in a certain way by spatial filtering and time series inversion during the multi-temporal InSAR processing and this is the advantage of multi-temporal InSAR processing compared to D-InSAR.

- Line 445: compared to the values recorded in previous studies. The references are necessary.
The references have been added to the revised manuscript. We also took the reviewer's suggestion of including a comparison (lake level/volume changes) in the revised manuscript. The contents are presented in Figure 10.

- Line 515: "in the northern two" to "in the two northern"
Corrected.

References

Berardino, P., Fornaro, G., Lanari, R., and Sansosti, E.: A new algorithm for surface deformation monitoring based on small baseline differential SAR interferograms, Geoscience and Remote Sensing, IEEE Transactions on, 40, 2375-2383, 2002.

Bian, D., Bian, B., La, B., Wang, C., and Chen, T.: The Response of Water Level of Selin Co to Climate Change during 1975-2008 (in Chinese), Acta Geographica Sinica, 65, 2010.

Brun, F., Treichler, D., Shean, D., and Immerzeel, W. W.: Limited contribution of glacier mass loss to the recent increase in Tibetan Plateau lake volume, Frontiers in Earth Science, 8, 495, 2020.

Chen, J., Wu, T., Zou, D., Liu, L., Wu, X., Gong, W., Zhu, X., Li, R., Hao, J., and Hu, G.: Magnitudes and patterns of large-scale permafrost ground deformation revealed by Sentinel-1 InSAR on the central Qinghai-Tibet Plateau, Remote Sensing of Environment, 268, 112778, 2022.

Cheng, G.: The mechanism of repeated-segregation for the formation of thick layered ground ice, Cold Regions Science and Technology, 8, 57-66, 1983.

Daout, S., Doin, M. P., Peltzer, G., Socquet, A., and Lasserre, C.: Large‐scale InSAR monitoring of permafrost freeze‐thaw cycles on the Tibetan Plateau, Geophysical Research Letters, 44, 901-909, 2017.

Deij, Y., Nima, J., Qianba, O., Zeng, L., and Luosang, Q.: Lake Area Variation of Selin Tso in 1975～ 2016 and Its Influential Factors, Plateau and Mountain Meteorology Research, 38, 2018.

Doin, M. P., Twardzik, C., Ducret, G., Lasserre, C., Guillaso, S., and Jianbao, S.: InSAR measurement of the deformation around Siling Co Lake: Inferences on the lower crust viscosity in central Tibet, Journal of Geophysical Research: Solid Earth, 120, 5290-5310, 2015.

Farinotti, D., Huss, M., Fürst, J. J., Landmann, J., Machguth, H., Maussion, F., and Pandit, A.: A consensus estimate for the ice thickness distribution of all glaciers on Earth, Nature Geoscience, 12, 168-173, 2019.

French, H. and Harbor, J.: 8.1 The Development and History of Glacial and Periglacial Geomorphology, Treatise on Geomorphology, Academic Press, https://doi.org/10.1016/B978-0-12-374739-6.00190-1, 2013.

French, H. M.: The periglacial environment, John Wiley & Sons2017.

Günther, F., Overduin, P. P., Yakshina, I. A., Opel, T., Baranskaya, A. V., and Grigoriev, M. N.: Observing Muostakh disappear: permafrost thaw subsidence and erosion of a ground-ice-rich island in response to arctic summer warming and sea ice reduction, The Cryosphere, 9, 151-178, 2015.

Guo, W., Liu, S., Xu, J., Wu, L., Shangguan, D., Yao, X., Wei, J., Bao, W., Yu, P., and Liu, Q.: The second Chinese glacier inventory: data, methods and results, Journal of Glaciology, 61, 357-372, 2015.

Guo, Y., Zhang, Y., Ma, N., Xu, J., and Zhang, T.: Long-term changes in evaporation over Siling Co Lake on the Tibetan Plateau and its impact on recent rapid lake expansion, Atmospheric research, 216, 141-150, 2019.

Hwang, C.-w., Cheng, Y. S., Yang, W. H., Zhang, G., Huang, Y. R., Shen, W. B., and Pan, Y.: Lake level changes in the Tibetan Plateau from Cryosat-2, SARAL, ICESat, and Jason-2 altimeters, Terr. Atmos. Ocean. Sci, 30, 1-18, 2019.

Kokelj, S. V. and Jorgenson, M.: Advances in thermokarst research, Permafrost and Periglacial Processes, 24, 108-119, 2013.

Lantuit, H. and Pollard, W.: Fifty years of coastal erosion and retrogressive thaw slump activity on Herschel Island, southern Beaufort Sea, Yukon Territory, Canada, Geomorphology, 95, 84-102, 2008.

Lei, Y., Yao, T., Bird, B. W., Yang, K., Zhai, J., and Sheng, Y.: Coherent lake growth on the central Tibetan Plateau since the 1970s: Characterization and attribution, Journal of Hydrology, 483, 61-67, 2013.

Li, X., Long, D., Huang, Q., Han, P., Zhao, F., and Wada, Y.: High-temporal-resolution water level and storage change data sets for lakes on the Tibetan Plateau during 2000–2017 using multiple altimetric missions and Landsat-derived lake shoreline positions, Earth System Science Data, 11, 1603-1627, 2019.

Liu, S., Guo, W., and Xu, J.: The second glacier inventory dataset of China (version 1.0) (2006-2011) [dataset], 10.3972/glacier.001.2013.db, 2012.

Mackay, J. R.: Downward water movement into frozen ground, western arctic coast, Canada, Canadian Journal of Earth Sciences, 20, 120-134, 1983.

Meng, K., Shi, X., Wang, E., and Liu, F.: High-altitude salt lake elevation changes and glacial ablation in Central Tibet, 2000–2010, Chinese Science Bulletin, 57, 525-534, 2012.

Pepe, A. and Lanari, R.: On the extension of the minimum cost flow algorithm for phase unwrapping of multitemporal differential SAR interferograms, IEEE Transactions on Geoscience and remote sensing, 44, 2374-2383, 2006.

Qiao, B., Zhu, L., and Yang, R.: Temporal-spatial differences in lake water storage changes and their links to climate change throughout the Tibetan Plateau, Remote Sensing of Environment, 222, 232-243, 2019.

Shiklomanov, N. I., Streletskiy, D. A., Little, J. D., and Nelson, F. E.: Isotropic thaw subsidence in undisturbed permafrost landscapes, Geophysical Research Letters, 40, 6356-6361, 2013.

Streletskiy, D. A., Shiklomanov, N. I., Little, J. D., Nelson, F. E., Brown, J., Nyland, K. E., and Klene, A. E.: Thaw subsidence in undisturbed tundra landscapes, Barrow, Alaska, 1962–2015, Permafrost and Periglacial Processes, 28, 566-572, 2016.

Sun, F., Ma, R., He, B., Zhao, X., Zeng, Y., Zhang, S., and Tang, S.: Changing Patterns of Lakes on The Southern Tibetan Plateau Based on Multi-Source Satellite Data, Remote Sensing, 12, 3450, 2020.

Tong, K., Su, F., and Xu, B.: Quantifying the contribution of glacier meltwater in the expansion of the largest lake in Tibet, Journal of Geophysical Research: Atmospheres, 121, 11,158-111,173, 2016.

Treichler, D., Kääb, A., Salzmann, N., and Xu, C.-Y.: Recent glacier and lake changes in High Mountain Asia and their relation to precipitation changes, The Cryosphere, 13, 2977-3005, 2019.

Zhang, G., Yao, T., and Kang, S.: Water balance estimates of ten greatest lakes in China using ICESat and Landsat data (in Chinese), Chin Sci Bull, 58, 2664-2678, 2013.

Zhang, G., Bolch, T., Chen, W., and Crétaux, J.-F.: Comprehensive estimation of lake volume changes on the Tibetan Plateau during 1976–2019 and basin-wide glacier contribution, Science of the Total Environment, 772, 145463, 2021a.

Zhang, G., Ran, Y., Wan, W., Luo, W., Chen, W., Xu, F., and Li, X.: 100 years of lake evolution over the Qinghai–Tibet Plateau, Earth System Science Data, 13, 3951-3966, 2021b.

Zhang, G., Yao, T., Shum, C., Yi, S., Yang, K., Xie, H., Feng, W., Bolch, T., Wang, L., and Behrangi, A.: Lake volume and groundwater storage variations in Tibetan Plateau's endorheic basin, Geophysical Research Letters, 44, 5550-5560, 2017.

Zhang, G., Yao, T., Xie, H., Yang, K., Zhu, L., Shum, C., Bolch, T., Yi, S., Allen, S., and Jiang, L.: Response of Tibetan Plateau's lakes to climate changes: trend, pattern, and mechanisms, Earth-Science Reviews, 103269, 2020.

Zhang, Y., Fattahi, H., and Amelung, F.: Small baseline InSAR time series analysis: Unwrapping error correction and noise reduction, Computers & Geosciences, 133, 104331, 2019.

Zhao, L. and Sheng, Y.: Permafrost and environment changes on the QinghaiTibetan Plateau (in Chinese), Science Press, Beijing, China2019.

Zhao, L., Hu, G., Zou, D., Wu, X., Ma, L., Sun, Z., Yuan, L., Zhou, H., and Liu, S.: Permafrost Changes and Its Effects on Hydrological Processes on Qinghai-Tibet Plateau (in Chinese), Bulletin of the Chinese Academy of Sciences, 34, 1233-1246, 2019.

Zhao, L., Zou, D., Du, E., Hu, G., Pang, Q., Xiao, Y., Li, R., Sheng, Y., Wu, X., Sun, Z., Wang, L., Wang, C., Ma, L., Zhou, H., and Liu, S.: Changing climate and the permafrost environment on the Qinghai-Tibet (Xizang) Plateau, Permafrost and Periglacial Processes, 10.1002/ppp.2056, 2020.

Zhu, L., Zhang, G., Yang, R., Liu, C., Yang, K., Qiao, B., and Han, B.: Lake Variations on Tibetan Plateau of Recent 40 Years and Future Changing Tendency (in Chinese), Bulletin of the Chinese Academy of Sciences, 34, 1254-1263, 2019a.

Zhu, L., Wang, J., Ju, J., Ma, N., Zhang, Y., Liu, C., Han, B., Liu, L., Wang, M., and Ma, Q.: Climatic and lake environmental changes in the Serling Co region of Tibet over a variety of timescales, Science Bulletin, 64, 422-424, 2019b.

Response to Reviewer #2

The manuscript "Contribution of ground ice melting to the expansion of Serling Co lake on the Tibetan Plateau" by Lingxiao Wang et al. is an interesting and original paper that aims to quantify the water volume contribution to the impressive change in water volume of Seling Co lake in Tibet. The work is original as it uses the ground deformation in areas within the watershed and prone to changes in ground ice volume to deduce the water release by ground ice melting. Three years of Sentinel-1 data from end of 2017 to end of 2020 have been processed by multi-temporal InSAR SBAS technique, leading to a decomposition between seasonal deformation associated mainly to freeze-thaw cycles and a three year trend that is mainly interpreted as decadal ice lense melting (for subsidence) or formation (for uplift). In situ core drillings support the existence of ice rich layers or ice lenses at depth between 2 and 8m, where seasonal deformation or pluri-annual subsidence is observed. Interpretation of GPR results also confirm the existence of ice in the same areas.

The paper is overall well written, present new and interesting data and an original way of quantifying the effect of permafrost degradation on lake level change. The endhoreic nature of this watershed area is also allows to test assumptions or models involved in water cycle quantification. It should be accepted for publication after addressing some comments below, that together lead to a major revision.

The authors are very grateful for the valuable comments and suggestions from the reviewer.

Detailed responses and revisions based on the comments are listed below.

InSAR processing and results

Ansari, de Zan et al. have shown that including only **very short temporal baseline interferograms leads to strong biais**, mostly in the form of a pluri annual subsidence. While my experience is that this bias appears mostly in crop areas, and should not be strong in this area of Tibet, it must be shown here that it is not the case (and I really believe that in Tibet you don't have such biais, or at least that what you see is real). The difficulty here is that freeze-thaw cycles lead to decreased coherence and high fringe gradient, such that interferograms with temporal baseline larger than 2 months are difficult to unwrap. You may find some methodology of how to overcome this in Daout et al., 2017 paper. A stack of numerous 1 year interferograms could also do the trick, provided that you can unwrap them.

Thank you very much for the valuable comments and suggestions.

1) **We tested different interferograms network schemes at the beginning of the work. A stack of numerous 1-year interferograms was also tested.**

According to the statistics on the interferometric coherence of intra-annual interferogram pairs, interferograms during the stable freezing and thawing months (end of Dec, Jan, Feb, Jul, Aug, beginning of Sep) usually have higher coherences than in the other months. Thus, The 1-year-span interferograms were only conducted during these months to exclude freeze-thaw cycles.

Two interferograms network strategies were compared.

Strategy #1, interferograms were generated by each SAR image with its two sequential acquisitions, which is the scheme used in this study.

Strategy #2, the 1-year-span interferograms were also included, in addition to the regular intra-annual interferograms used in strategy #1.

The following Figure R1 compares the applicability of the above two strategies in constructing interferogram networks. The interferometric coherence is lower in the months experiencing freeze/thaw transitions than in Jan-Feb and Jul-Aug, but it is maintained above an acceptable level (the averaged coherence of each interferogram above 0.7). The study area doesn't face strong decorrelation taking the interferograms network strategy #1.

However, 1-year interferograms have much lower coherence than interferograms experiencing freeze/thaw transitions.
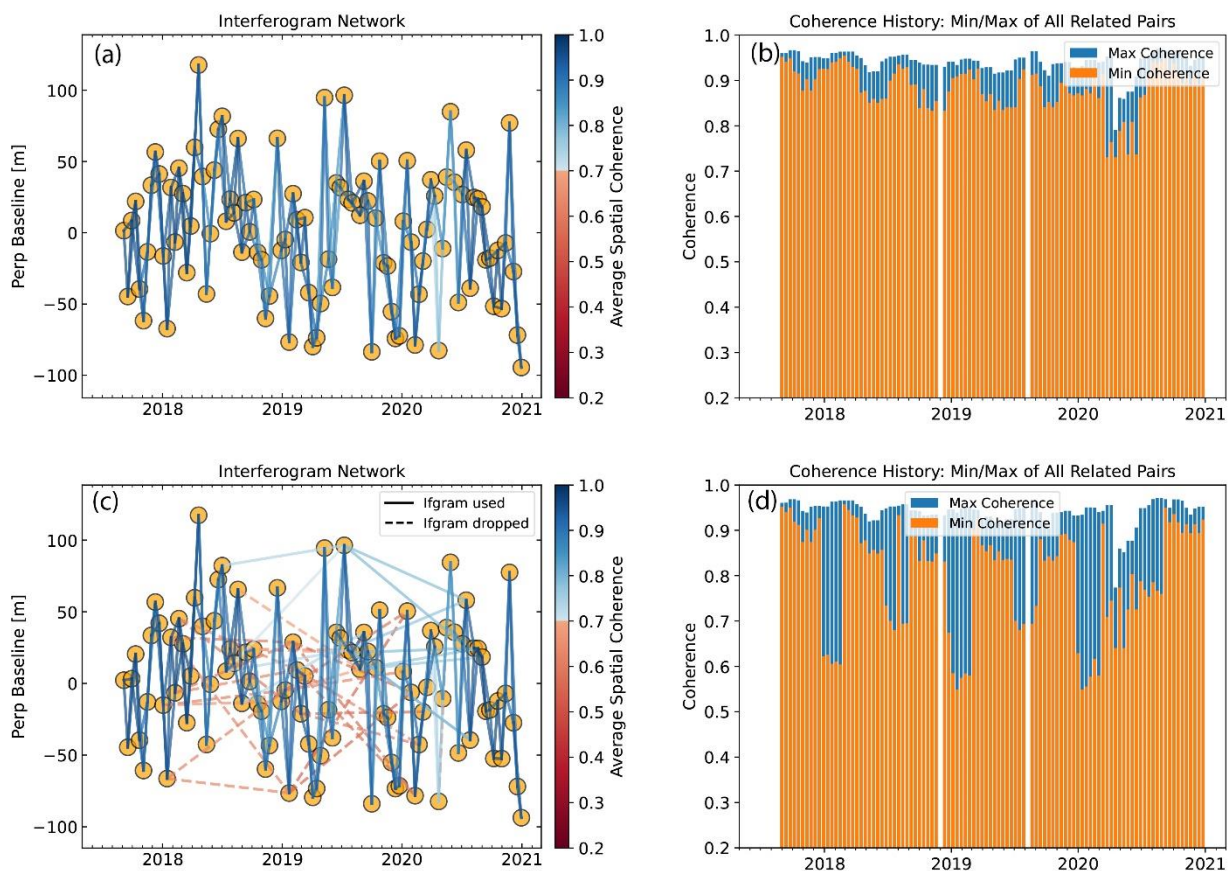
Fig. R1 The upper panel (a-b) shows the interferometric coherence of network strategy #1 and the bottom panel (c-d) shows the results of strategy #2. The extent of interferograms in strategy #2 is slightly smaller than that in strategy #1 (The north-south direction is 40 km smaller). The left panel (a)(c) shows the network of interferograms for deformation time series estimation, color-coded by the average coherence of the interferograms. Circles represent the acquisition dates, and lines represent the interferograms. Solid lines are the interferograms used for time-series estimation, and dashed lines are the interferograms ignored in the time-series estimation. The left panel (b)(d) shows the average coherence of all related pairs for each SAR acquisition date.

2) The qualities of interferograms have been visually examined.

Fig. R2 displays fourteen interferograms together with their unwrapped phases in upstream of Zhajiazangbu,

where widespread continuous permafrost is present. The interferograms for each month of the year are presented. In addition to 24-days interferograms, displays two 1-year interferograms of 20180702-20190709 and 20190122-20200129 are also displayed. On the 1-year interferogram pair, low interferometric coherence is accompanied by unwrapping errors. We didn't observe distinct unwrapping errors among the 24-days interferograms in the land regions (excluding water and glacier) and permafrost-induced deformation is clear on several interferograms. The atmospheric distortions are also strongly visible on several interferograms.
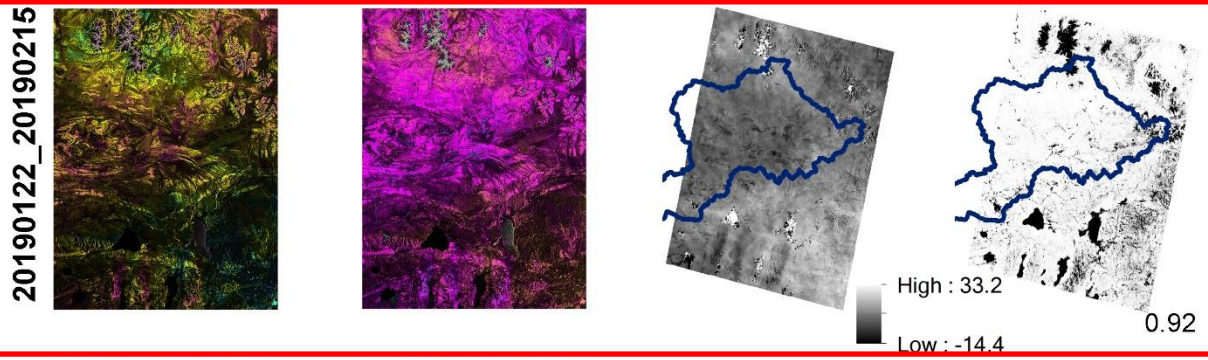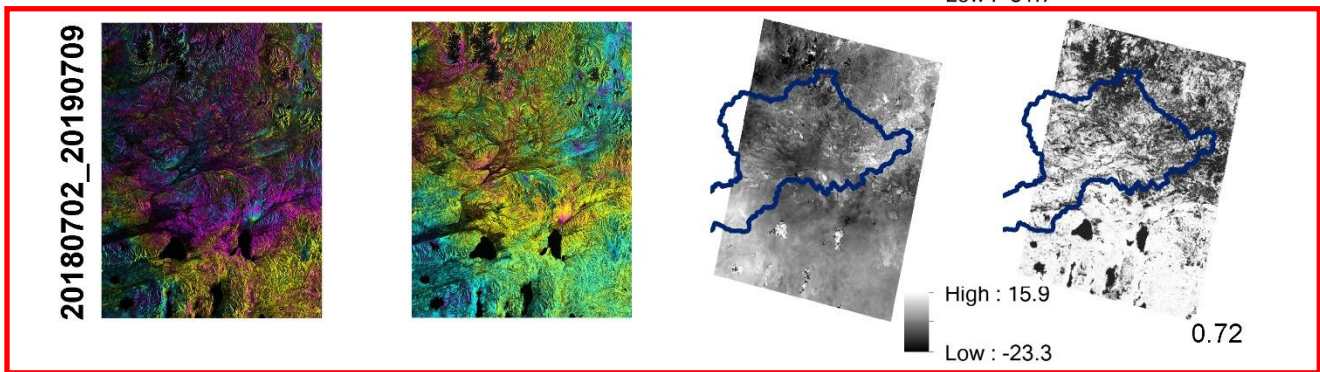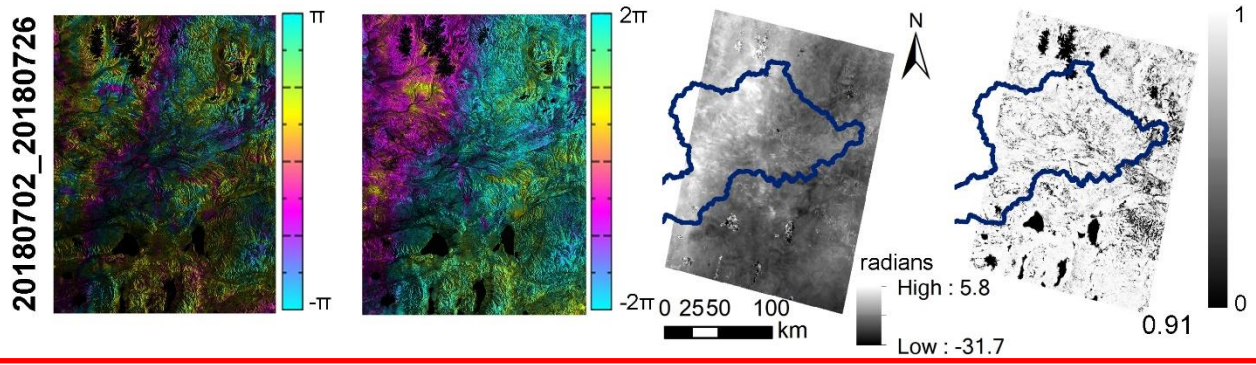
filtered interferogram   unwrapped phase   geocoded unwrapped phase interferometric coherence

filtered interferogram   unwrapped phase   geocoded unwrapped phase interferometric coherence
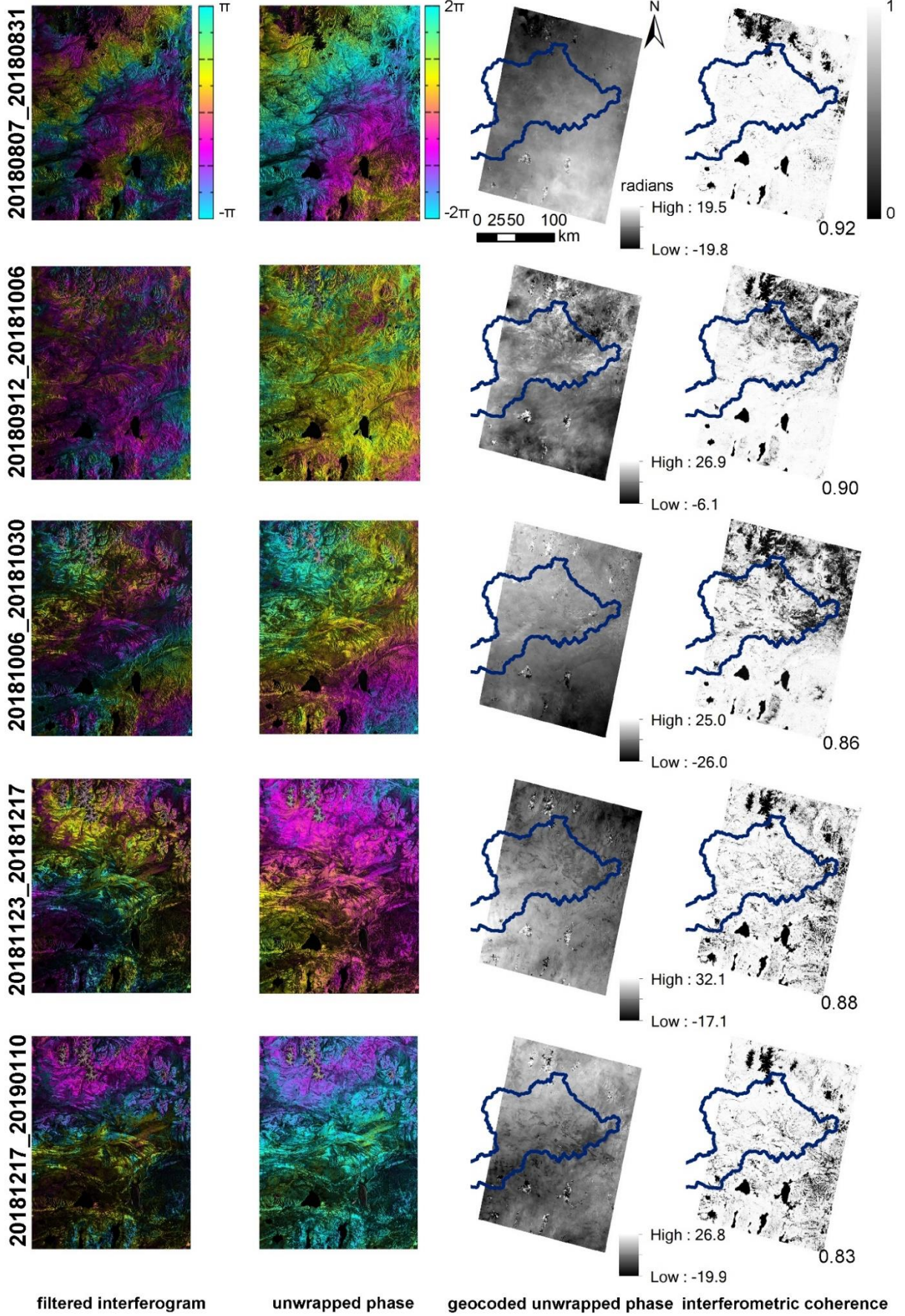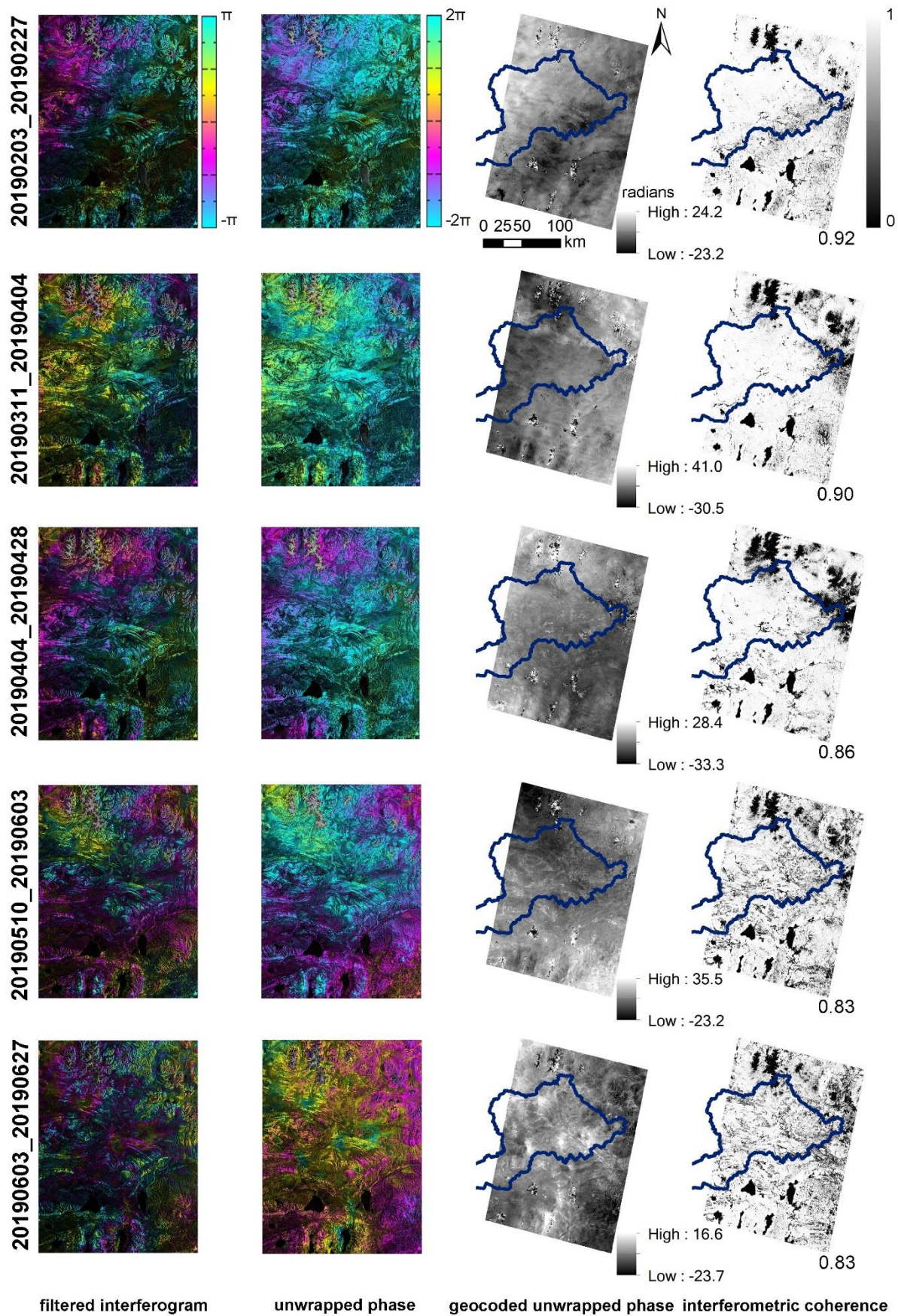
Fig. R2 Examples of 24-days interferograms. The value below the interferometric coherence map labels the averaged value of the map. The decorrelated area in the north is Mt. Geladandong.

3) **The unwrapping error corrections were applied before network inversion to further reduce unwrapping errors (Zhang et al., 2019).** The unwrapping error correction is conducted by bridging reliable regions. The bridging scheme can be described as a three-step procedure for each interferogram. The first step is to identify reliable regions using the connected component information provided by SNAPHU (Chen and Zebker, 2002). The second step is to construct directed bridges to connect all reliable regions using the minimum spanning tree (MST) algorithm minimizing the total bridge length. The third step is to estimate for each bridge the integer-cycle phase offset between the two regions. This is similar to region assembly in the secondary network in phase unwrapping (Chen and Zebker, 2002), but in the tertiary level.

Based on the experiments above, we decided to adopt the scheme that interferograms were generated by each SAR image with its two sequential acquisitions.

Unwrapping: Given the difficulty to unwrap permafrost related InSAR signals, you should show a few examples of 24 days interferograms in an appendix together with their unwrapped counterparts. Can you please use network misclosure (Lopez quiroz et al., 2009) during network inversion to quantify the amount of possible unwrapping error? Please cite the Minimum Cost Flow algorithm used here. The time series shown in the paper, with respect to the reference point quite far away, appear extremely smooth in time, where atmospheric contribution of two points 100km apart should, even in Tibet at its very high elevation, be of at least a cm up to a few cm. Please explain what smoothing you used (I guess embedded in MintPy).

Thank you very much for the valuable suggestion.

1) **The examples of 24 days interferograms are shown in the above Fig. R2.**

2) **Taking the reviewer's suggestion, we also quantitatively evaluate the amount of possible unwrapping error during the network inversion using the idea of network misclosure, but slightly different from (Lopez-Quiroz et al., 2009).** The methods are stated in section 3.3.1 SBAS-InSAR processing ii) Deformation time series estimation as follows:

Two indicators evaluated the quality of unwrapped phases and inverted raw phase time series: the phase closure of interferogram triplets and temporal coherence. The phase unwrapping algorithms add integer number of 2π phase jumps to recover the unwrapped phase. Interferometric phase noise and discontinuities among different coherent regions may lead to wrong 2π jumps added to the phase field known as unwrapping error. Unwrapping errors can bias the estimated time series. For an interferogram triplet ($\Delta\phi^{ij}$, $\Delta\phi^{jk}$ and $\Delta\phi^{ik}$), unwrapping errors introduce a nonzero integer component C_{int}^{ijk} in the closure phase C^{ijk}. Therefore, the number of interferogram triplets with nonzero integer ambiguity T_{int} can be used to detect unwrapping errors:

$$C^{ijk} = \Delta\varphi^{ij} + \Delta\varphi^{jk} - \Delta\varphi^{ik} \tag{2}$$

$$C_{int}^{ijk} = \frac{C^{ijk} - wrap\,(C^{ijk})}{2\pi} \tag{3}$$

$$T_{int} = \sum_{i=1}^{T} \left(C_{int}^{ijk} \neq 0 \right) \tag{4}$$

where $\Delta\varphi^{ij}$, $\Delta\varphi^{jk}$ and $\Delta\varphi^{ik}$ are the three unwrapped interferometric phases generated from the SAR acquisitions at t_i, t_j and t_k, respectively; wrap is an operator that wraps each input number into $[-\pi, \pi)$; and T is the number of interferogram triplets. A triplet without unwrapping errors has $C_{int}^{ijk} \equiv 0$.

The second index, temporal coherence, represents the consistency of the time series with the network of interferograms (Pepe and Lanari, 2006):

$$\gamma_{temp} = \frac{1}{M} \left| H^T \exp\left[j(\Delta\phi - A\hat{\phi}) \right] \right| \tag{5}$$

where (for N SAR images and M interferograms) $\Delta\phi$ is the unwrapped interferometric phase; A is the $M \times (N - 1)$ design matrix indicating the acquisition pairs used for interferograms generation (consisting of -1, 0 and 1 for each row with -1 for the reference acquisition, 1 for the secondary acquisition and 0 for all other acquisitions (Berardino et al., 2002)); $\hat{\phi}$ denotes the estimated time series; H is an M×1 all-ones column vector; and j is the imaginary unit.

Temporal coherence varies from 0 to 1: pixels with values closer to 1 are considered reliable, whereas pixels with values closer to zero are considered unreliable. A threshold of 0.7 is recommended to be used for a dense network of interferograms. In this study, we used a threshold of 0.85; the pixels with temporal coherence below this threshold were masked from the final result.

The quantitative evaluation results are presented in Section 4.4.2 Uncertainties and accuracies of deformation as follows.

Two indicators evaluated the quality of unwrapped phases and inverted raw phase time series: the phase closure of interferogram triplets and temporal coherence. Fig. 11 in the revised manuscript shows the spatial distribution of the number of interferogram triplets with nonzero integer ambiguity T_{int} (Eq(4)), with the histogram illustrating the distribution of T_{int} values within the Selin Co watershed excluding glaciers and water bodies. The areas having T_{int} smaller than three take part 95% of the watershed, while 72.3% of the watershed has T_{int} value of zero (no wrapping error on all the interferograms). The T_{int} evaluated the quality of original interferometric unwrapped phases, and the unwrapping errors could be further reduced by bridging reliable regions before network revision (Zhang et al., 2019).
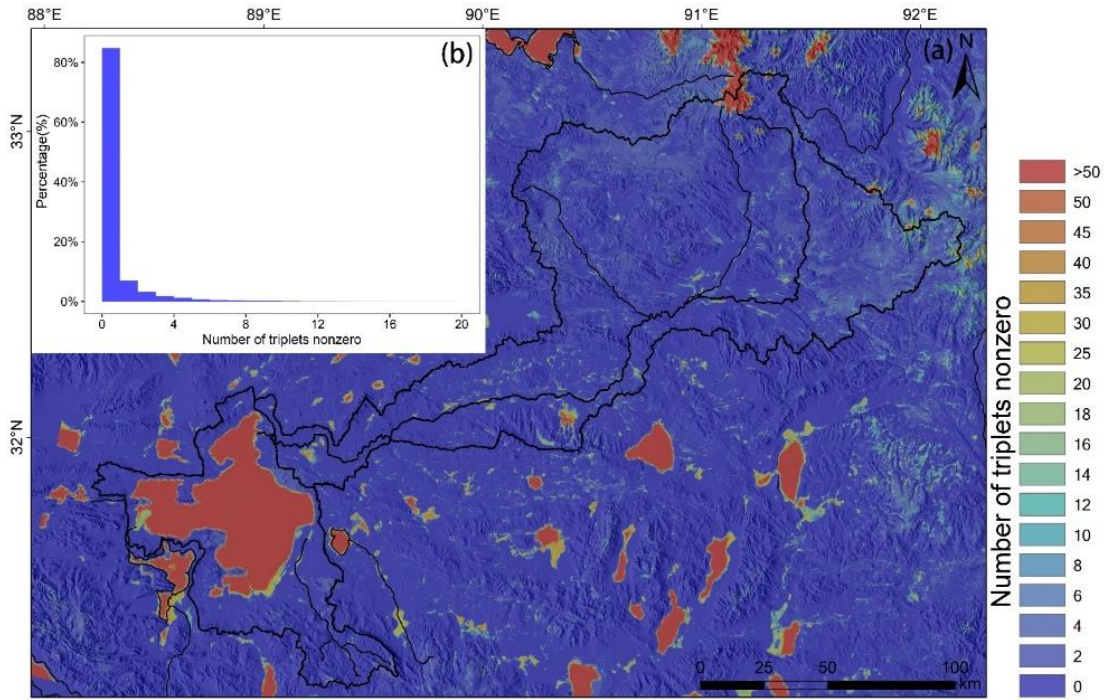
Figure 11 (a) Map of the number of interferogram triplets with nonzero integer ambiguity T_{int} (Eq(4)), (b) histogram illustrating the distribution of T_{int} values within the Selin Co watershed excluding glaciers and water bodies.

Fig. 12 shows the spatial distribution of temporal coherence (Eq.(5)), which is used to evaluate the quality of raw phase time series. 99.0% of the watershed has temporal coherence higher than 0.8, 98.1% has temporal coherence higher than 0.85, 96.0% has temporal coherence higher than 0.9, and 89.1% has temporal coherence higher than 0.95.
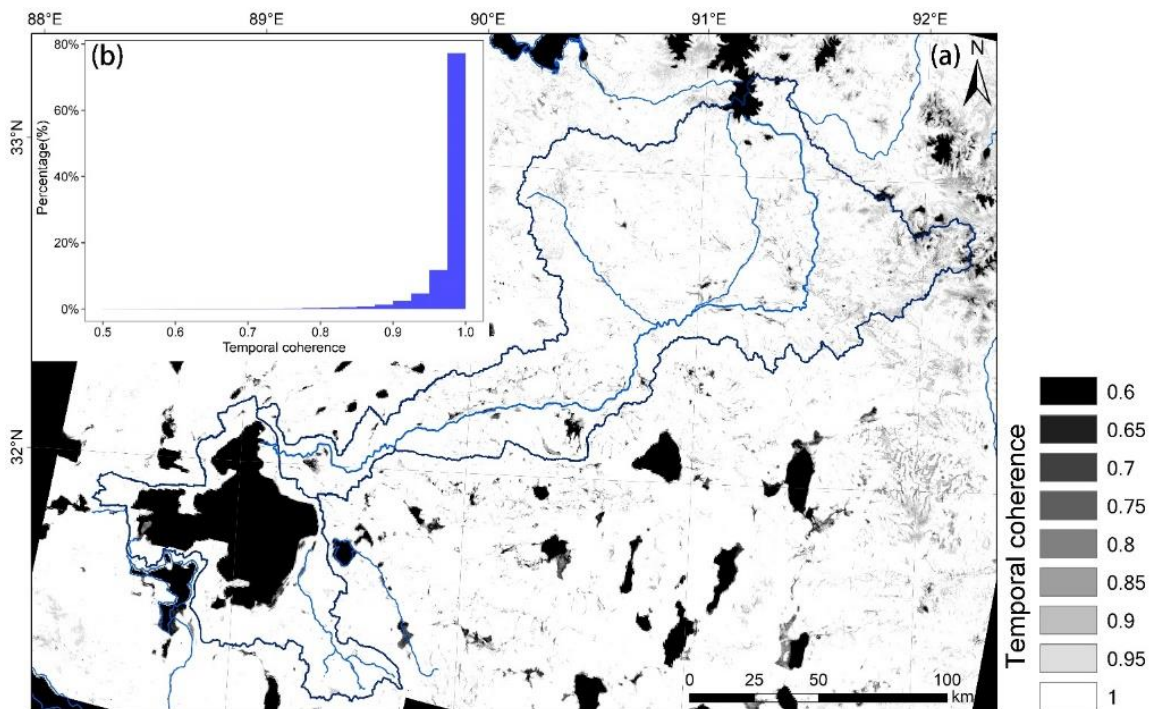
Figure 12 (a) Map of temporal coherence (Eq(5)), (b) histogram illustrating the distribution of temporal coherence values within the Selin Co watershed excluding glaciers and water bodies.

3) **The Minimum Cost Flow algorithm has been cited in the revised manuscript.** It has been cited in the revised manuscript that "To unwrap the differential phase, the SNAPHU Minimum Cost Flow (MCF) phase unwrapping algorithm (Chen and Zebker, 2002) was applied."

4) **Regarding the selection of reference point and residual atmospheric distortions**, we realized that it is inappropriate to put the reference point such far away from the studying watershed giving consideration to atmospheric distortions and tectonic movements on the TP. We selected a reference point near the boundary of Selin Co watershed not affected by permafrost in dry and flat terrain. The residual phases from atmospheric distortions and tectonic movements on the TP are difficult to remove completely in such a large-scale extent. However, the effect could be reduced by setting the reference near the study area. Taking several helpful suggestions of the reviewer, we have reprocessed the network inversion and time series estimation. After this reprocessing, the residual distortions (e.g., large area of slight uplift in the previous manuscript) have been reduced, or at least reduced in the studying watershed. The results are correspondingly updated through the revised manuscript.

5) **The time series appear smooth because we applied a 3-size moving window filter to the deformation time series.** We stated that "To minimize the effects of extreme values, we also applied a 3-size moving window filter to the deformation time series." in the section "3.3.2 Extraction of the periodic (seasonal) amplitude and long-term rate" in the original manuscript. To be clear, we have moved this sentence to the end of section "3.3.1 SBAS-InSAR processing" in the revised manuscript. The following Fig. R3 shows the deformation time series of drilling sites before (small black dots) and after (large green dots) 3-size moving window filtering.
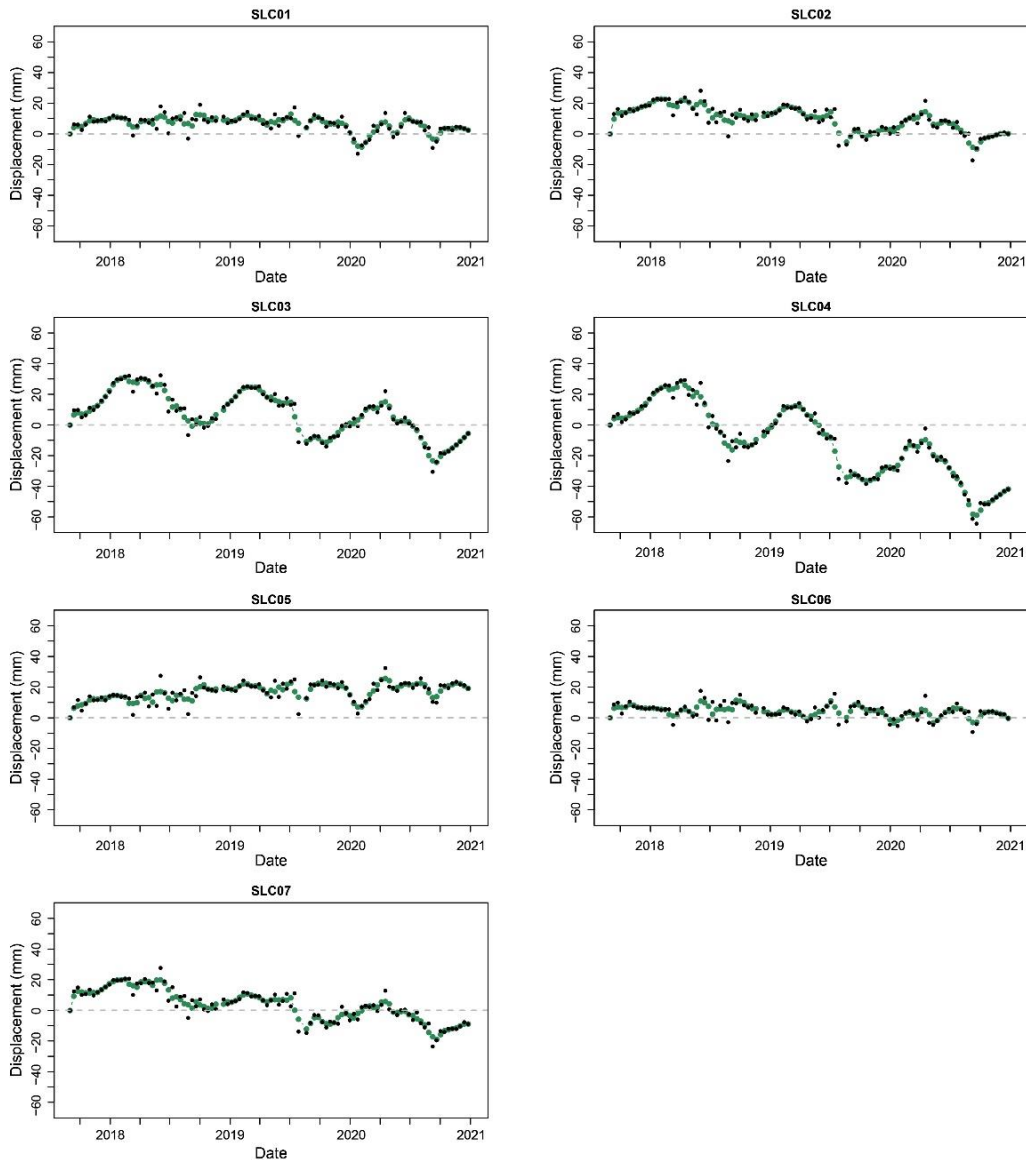
Fig. R3 Deformation time series of drilling sites before (small black dots) and after (large green dots) 3-size moving window filtering.

The discussion of possible **uplift and hence permafrost aggradatio**n could be improved. First of all, one can see on Figure 6 an E-W and N-S trend in velocity in areas not affected by permafrost, the trend resulting in apparent uplift on the NE corner. Deramping here should be evaluated on pixels not affected by permafrost (otherwise the ramp that is removed is affected by subsidence). A display of the seasonal amplitude and velocity field of the whole study area could help assess this trend. On Fig5, inserting panels with zooms on the amplitude and trend plus the location of time series would help the reader. The patterns associated with uplift could then be visualized in correspondence with the optical image. If the uplift is due to permafrost aggradation, it should also have a seasonal component as ice freezing only happens in winter/spring. Please note that sedimentation cannot lead to uplift, as it only destroys coherence. InSAR only follows the displacement of targets that remain coherent between successive acquisitions.

Thank you very much for the valuable advice. Taking several helpful suggestions from the reviewer, we have reprocessed the deformation time series estimation. We have also selected a larger sector and part of which is covered by both orbit 150 and orbit 48, to assure that the deformation pattern appears on both of the results from the two tracks. Taking the reviewer's suggestion, the zoomed seasonal amplitude and velocity are displayed along with an optical image and DEM overlapped on the hill shade for a better interpretation of the results. The locations of the sites are labeled on all the subfigures. These sites all have high interferometric coherence and T_{int} value of zero (no wrapping error on all the interferograms). Due to a lack of field investigation, it is hard to attribute it absolutely to permafrost aggradation or the rise of the groundwater table or sedimentation. Thus, we only presented the uplift signal and discussed this phenomenon in the discussion section in the revised manuscript.

The discussion of the uplift signal has been adjusted and moved to section "5.1 Uplift displacement signal" as follows.

5.1 Uplift displacement signal

In addition to widespread subsidence detected in upstream of Zhajiazangbu of the continuous permafrost environment, the uplift signal was also observed in the sporadic permafrost environment in the middle stream of the Zhajiazangbu subbasin, also near some drained ponds. Fig. 13 shows a sector (location marked in red rectangle in Fig. 1, 6–7), in which both subsidence and uplift signals are detected. The mean annual air temperature is -2.0°C, calculated based on ERA5-Land air temperature hourly reanalysis data during 2017–2020. For a better interpretation, Landsat optical image and elevation overlapped on the hillshade were also presented. The spatial distribution pattern of deformation aligns with landscape and topography very well. Large seasonal amplitude only appears in the vegetated and wet area, which indicates the water storage in the active layer in a certain way. Uplift signals are generally at the slope feet. Fig. 13(e)–(h) displays the deformation time series of four sites s1-s4 from high elevation to low elevation. Site s2 is stable, viewing from seasonal amplitude and long-term deformation velocity. The subsidence of site s3 is the result of ground ice melting, confirmed by the large periodic seasonal amplitude caused by frost heave and thaw subsidence in the active layer. The uplift signals of site s1 and site 4 are worth exploring, especially site s4. Site s4 has a possibility of being related to ground ice aggradation since it also exhibits moderate seasonal amplitude, but it is more likely related to sediment accumulation or groundwater table rise regarding its location.
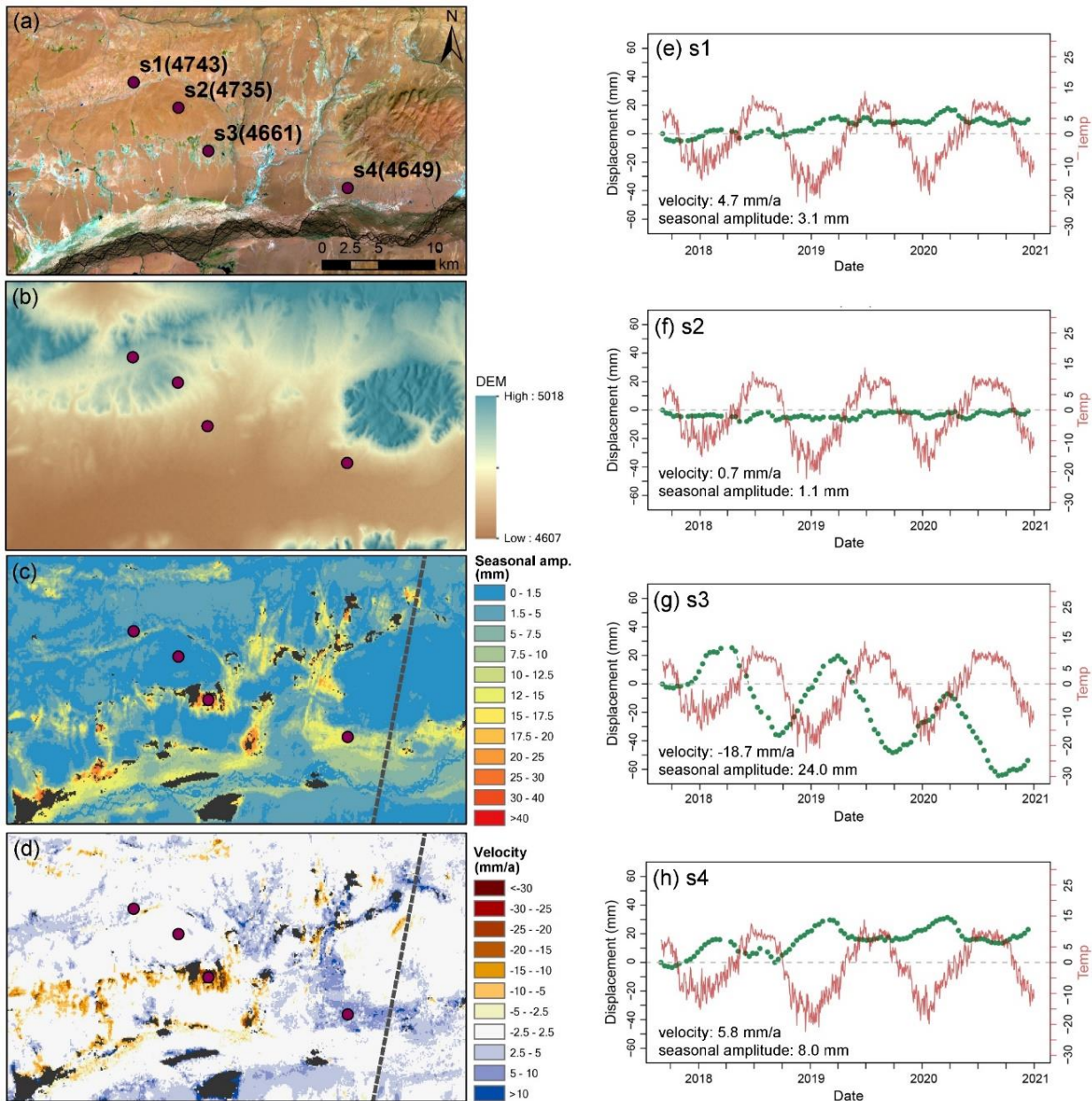
Figure 13 Deformation characters. This sector is marked with the red rectangle in Fig. 1 and 7-8. (a) Landsat 8 image (red: SWIR1, green: NIR, blue: red). (b) DEM overlapped on the hillshade, which is calculated using DEM with the Sentinel-1 incidence angle and azimuth angle. (c)(d) are seasonal deformation amplitude and long-term deformation velocity, respectively. The grey dashed line delineates the track boundary of orbit 150. (e)-(h) are deformation time series of marked sites. The elevetation (m a.s.l.) of the sites are labeled in brackets in subfigure (a). Air temperature in red color is from ERA5-Land air temperature reanalysis data. Deformations are in the LOS direction.

Previous research normally focuses on the thaw subsidence signal on the TP, and less attention has been given to the uplift signal. Some of the uplift signals might be related to deposition or the rise of the groundwater table. Some of the uplift signals might be caused by ground ice aggradation. A sufficient water supply accompanied by strong evaporation (cooling effect, energy is taken away) might facilitate the upward freezing of previously unfrozen (or seasonally frozen) sediment. Ground ice aggradation is slightly surprising in the overall warming climate of the study area. However, the upward freezing of previously unfrozen (or seasonally frozen) sediment is

still possible and may occur because of sediment accretion (e.g., deltaic and alluvial sedimentation) (French, 2017). A previous study (Daout et al., 2020) also detected a complex deformation signal in the permafrost on the northeastern TP and hypothesized that the uplift deformation in lowland regions was caused by excess meltwater pooling, which triggered an increase in the segregation of ice near the permafrost table. On the TP, new permafrost forming is detected on the exposed bottom of Zonag Lake (Zhang et al., 2022). Thus, on the TP, it might be common for degradation and aggradation of ground ice to both occur in permafrost environments, with degradation representing the dominant pattern and aggradation existing in local areas. Currently, most studies focus on permafrost subsidence signals, and few studies have studied permafrost ground ice aggradation and the causes of uplift signals in local environments. Nevertheless, the uplift signals in the permafrost environment on the TP are worthy of additional research, and further details on the Selin Co basin are expected to be unveiled and supplemented by the next field survey.

The footprint of the two tracks, the satellite heading and LOS direction should be shown on a figure. Please put also the LOS direction on the amplitude and velocity maps, even if you assume vertical displacement (which is decent here). Please state line 155 if you processing ascending or descending tracks.

Thank you for the suggestion.

1) **The descending tracks were emphasized.** It has been stated in the revised manuscript that "In total, 95 acquisition dates for descending orbit 48 and 100 acquisition dates for descending orbit 150 from September 2017 to December 2020 were processed."

2) **The tracks of orbit 150 and orbit 48 are marked in Fig. 1. Appendix Fig. A2 also presented the results from orbit 48 and 150, respectively.**
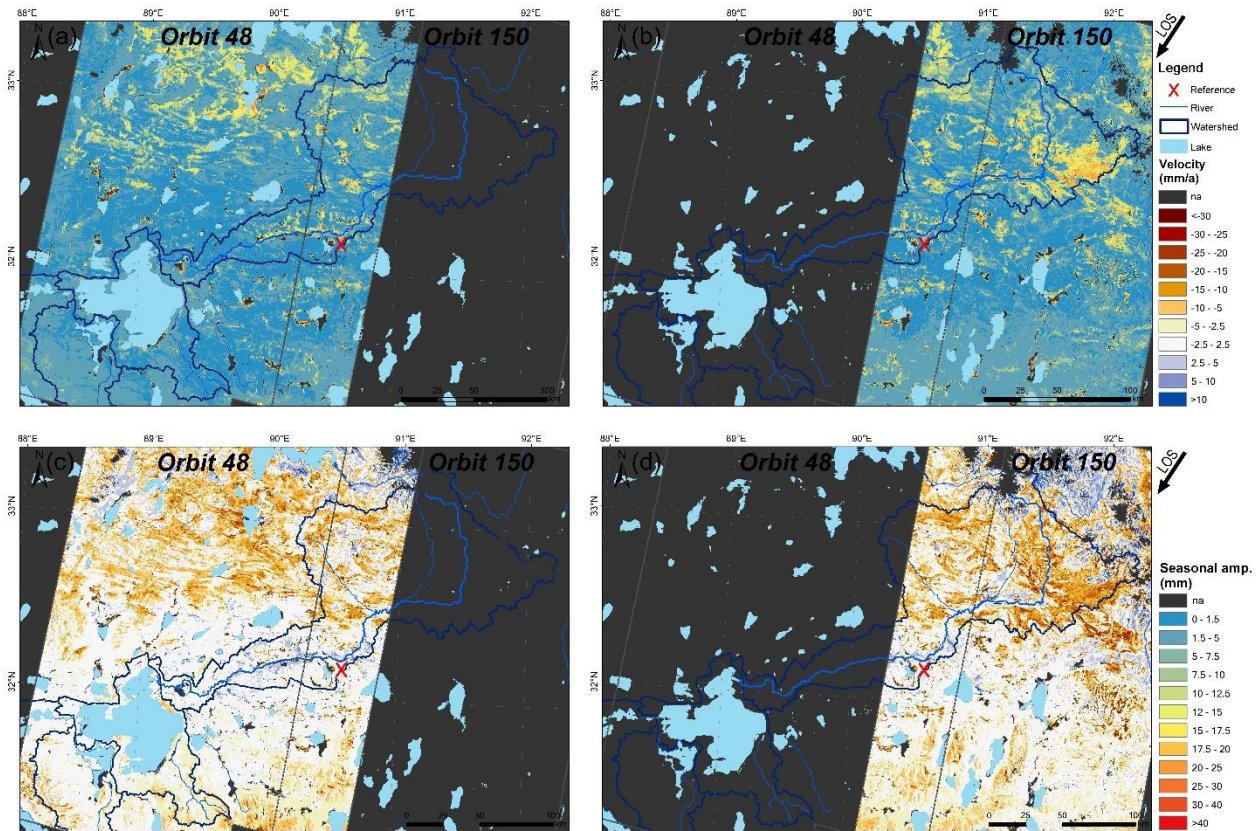
Fig. A2 Map of the periodic (seasonal) amplitude (a)(b) and long-term velocity (c)(d) retrieved from orbit 48 (a)(c) and orbit 150 (b)(d), respectively, all are in the satellite LOS direction.

3) **The satellite heading and LOS direction have been marked** in Figure 6 (seasonal amplitude) and Figure 7 (deformation velocity) in the revised manuscript.
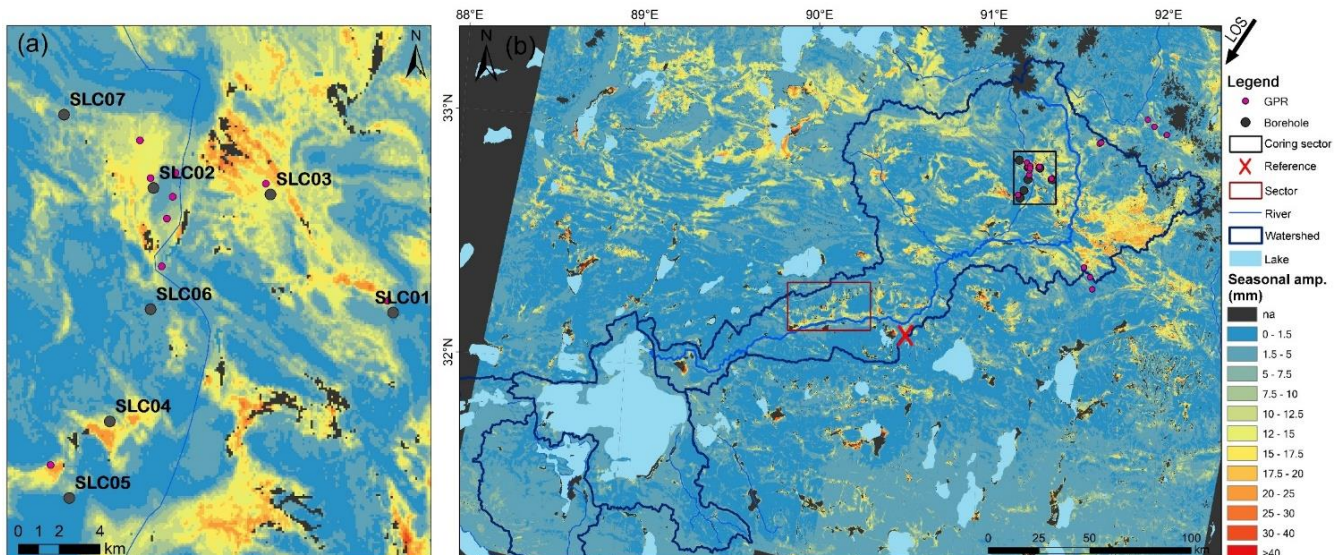
Figure 6 Map of the periodic (seasonal) amplitude in the satellite LOS direction. Subfigure (b) shows an enlarged view of the coring area (black sector in subfigure (a)). Dark grey colored "na" means the information could not be retrieved because of no data or decorrelation.
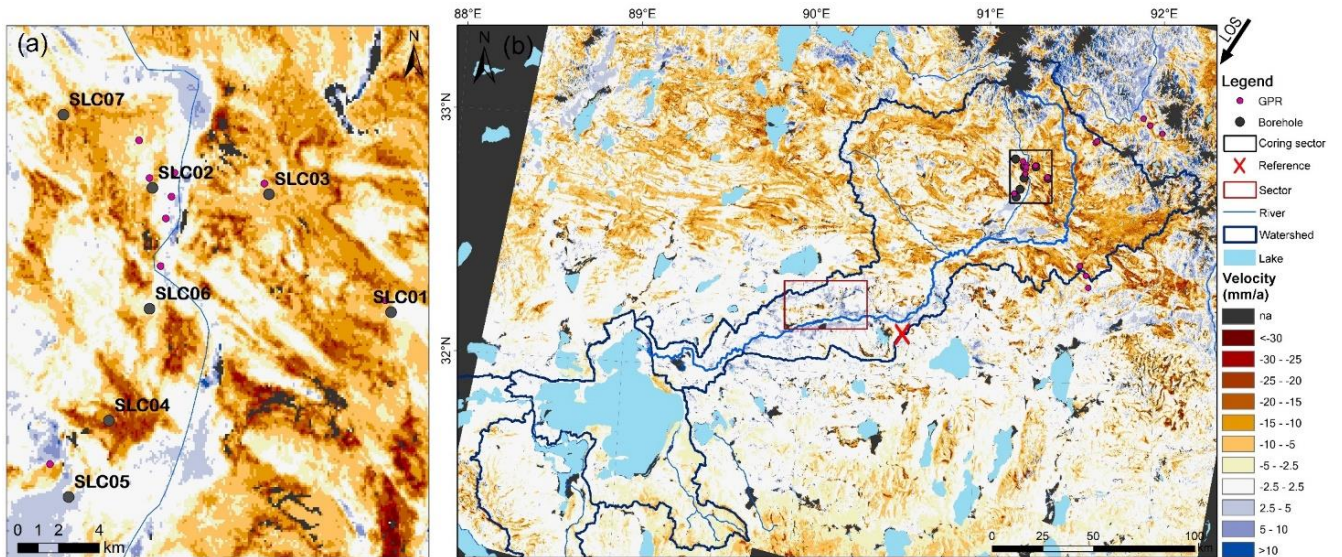
Figure 7 Map of the inter-annual deformation velocity in the satellite LOS direction. Subfigure (b) shows an enlarged view of the coring area (black sector in subfigure (a)). Dark grey colored "na" means the information could not be retrieved because of no data or decorrelation.

The **uncertainty on velocity maps is completely wrong** and should be recomputed or deleted (it is at best of the order of a mm/yr for an evaluation with 100 dates spread over 3 years, and with a reference point located at distance of about 100km). The evaluation cannot be made on smoothed time series unless you consider then temporally correlated noise. It does not then include possible biais or unwrapping error, but that's fair enough.

Thank you for your comment. We have removed this map in the revised manuscript because the uncertainty on velocity is calculated on smoothed time series and doesn't consider the residual errors (unwrapping error, phase ramps, atmospheric distortions). Instead, taking the reviewer's suggestion, we used the network misclosure to evaluate the uncertainties and accuracies of unwrapping error and raw phase time series estimation.

Other comments:

Coring was performed in autumn. Please indicate implication: end of thaw period. Is this why you can conclude from coring that you can measure the depth of the active layer or top of permafrost table? Active layer is by definition evolving through time. Please clarify your methodology here. A sketch of expected permafrost or active layer features with depth would be welcome as I am not sure I really understand the relation between Table 2 permafrost table and "dev of ground ice" columns.

Thank you very much for the comment and suggestion. Yes, from coring, the location of the permafrost table (active layer thickness) and the development of ground ice were described, which provides a sketch of permafrost features. Taking the reviewer's suggestion and to be clear, we have modified the statements as follows, "We conducted a field investigation of the permafrost in the study area in October 2019. Seven boreholes deeper than 20 m were drilled, and ground-penetrating radar (GPR) surveys were carried out in the upstream section of the Zhajiazangbu subbasin (locations are marked in Fig. 1). The survey was performed at the end of the thawing period, allowing us to estimate the maximum thawing depth and the location of the permafrost table. The permafrost table was estimated from the cores of the boreholes, and the development of ground ice was described

as well. Descriptions of the boreholes are provided in Table 2, and field photographs of the cores at borehole sites SLC01 and SLC04 are shown in Fig. 2."

Assumption is here done that total settlement is due to ice melting at the top of the permafrost table. Can you discuss a possible contribution of ice/water present in the soil porosity? Would then settlement be less per unit of ice melting, at least in a drained setting?

Thank you very much for the comment. We understand that the reviewer considers that the settlement might be less per unit of ice melting. Based on our experiences from coring in the Selin Co watershed and on the TP, the permafrost layer just below the permafrost table always contains ground ice higher than 50% in volume (Cheng, 1983; Zhao and Sheng, 2019). So we assumed that the amount of the surface settlement would release the same amount of ground ice caused by compressing the thawing ice-rich permafrost layer. To be clear, we have added these statements in the Introduction section.

Line 372-376: Replace text by a figure showing a density plot of seasonal amplitude versus velocity.

Thank you very much for this suggestion. We have added a density plot in this part as follows. The manuscript states that "Fig. 8 shows a density plot of the seasonal amplitude versus the deformation rate. Subsidence in the Selin Co watershed was normally between 5 and 20 mm/a (see the statistical details in Table 8) but reached 50 mm/a in certain regions, reflecting highly excessive volumes of ice and rapid ice loss in this region. The seasonal amplitude ranged between 0 mm and 60 mm within the watershed area. In the Zhajiazangbu subbasin with extensive permafrost, among the areas with deformation rates greater than 2.5 mm/a, 0.1% of them had seasonal amplitudes greater than 30 mm, 2.2% had amplitudes between 20 mm and 30 mm, 24.1% had amplitudes between 10 mm and 20 mm, 23% had amplitudes between 5 mm and 10 mm, and 50.6% had amplitudes of less than 5 mm; overall, the average seasonal amplitude was 6.9 mm."
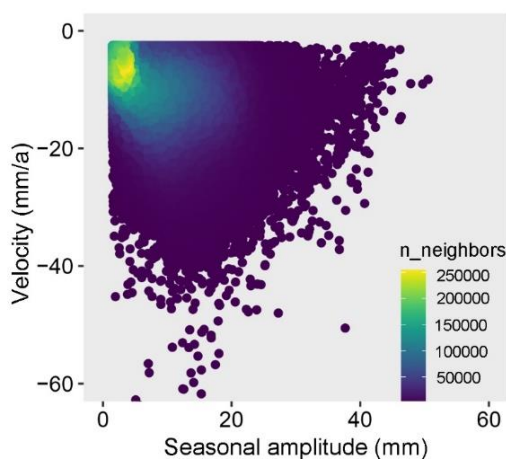

Figure 8 Distribution of the LOS seasonal amplitude versus the LOS deformation velocity within the Selin Co watershed, in all 6.57 $\times 10^5$ valid pixels.

*paragraph 4.2.3: show a zoom of velocity and amplitude map in areas of drillings and GPR, with annotated core numbers

Thank you very much for the suggestion. The zoomed figures of velocity and amplitude in the coring sector have been added in above Fig. 6 and Fig. 7, with the core number annotated.

Appendix Fig. A3 also provides a larger deformation map covering the field investigation region.
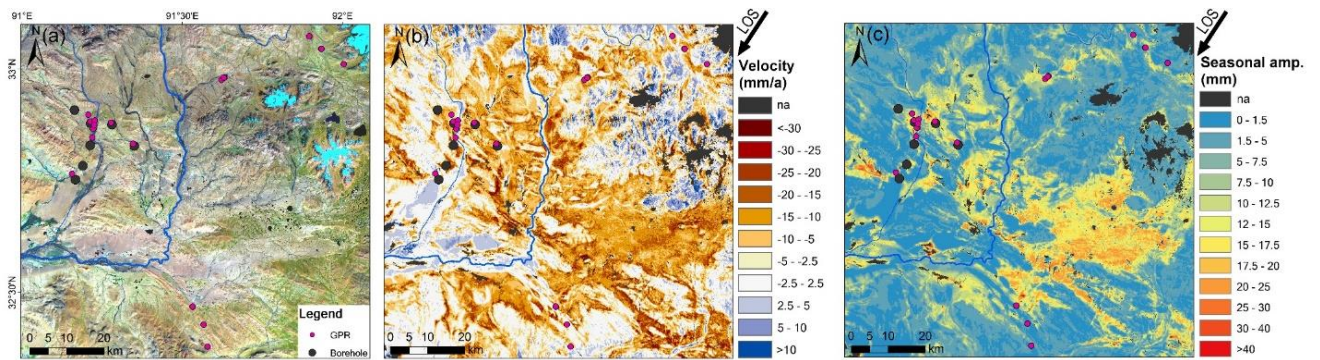
Fig. A3 Maps of the GPR and borehole regions, (a) Landsat 8 image acquired in October 2020 (red: SWIR1, green: NIR, blue: red), with GPR and borehole sites marked, (b) long-term deformation velocity, (c) seasonal deformation amplitude.

Figure 9 : the unit is strange. I suggest to drop the figure as I guess it is simply the velocity multiplied by pixel size. The unit should stay as a velocity as it is a volume per unitsize per unit time.

Thank you for the comment. Yes, it is the vertical velocity multiplied by pixel size, but masked out regions having large slopes and small seasonal amplitude. We agreed with the reviewer that that unit should be velocity. The unit in the figure has been corrected. The figure has been modified and shown as follows.
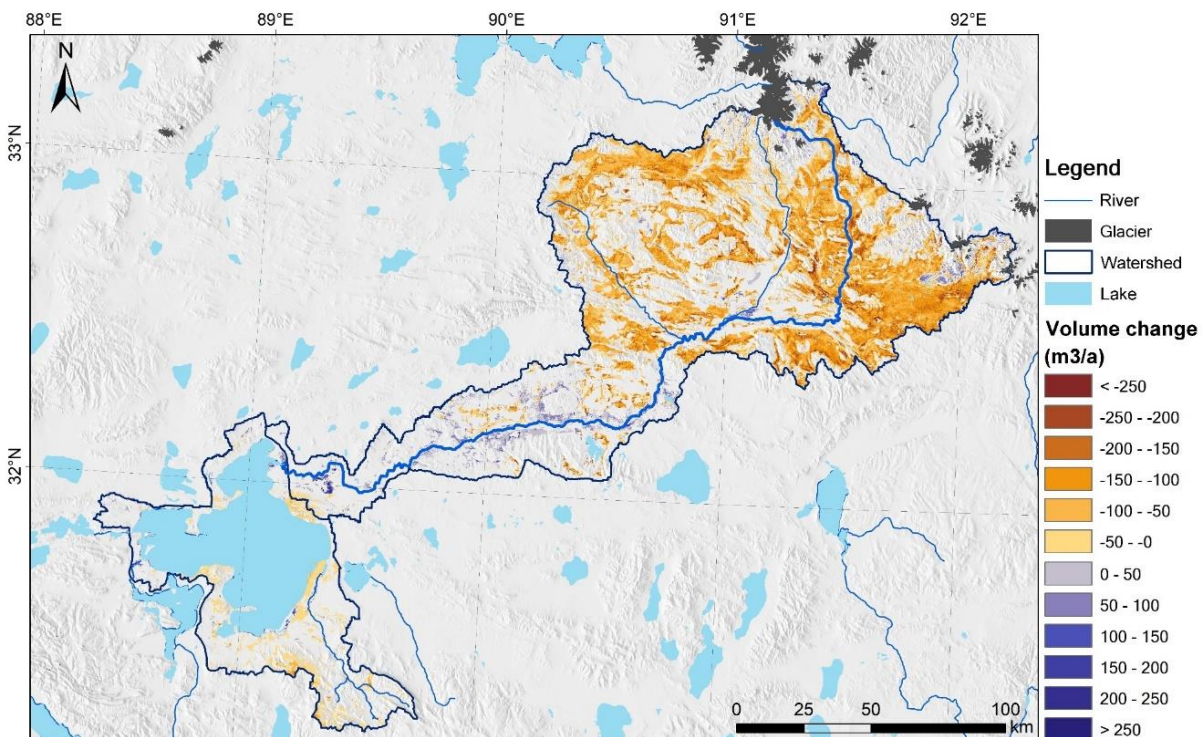
Figure 9 Map of the potential ground ice melting water supply. The grid color represents the grid cell's yearly ground ice melting water supply volume, with negative values indicating ground ice loss and meltwater release.

Comments on various parts of the manuscript

Thank you very much for the advice. Accordingly, we have modified the statements in Introduction as "The entire Selin Co watershed covers a drainage area of 4.4×10^4 km^2, 18 times the lake surface. Accordingly, a lake water level increase of 0.2 m/a corresponds to at least 1 cm/a of water collected uniformly over the whole watershed area (neglecting evaporation)….according to this permafrost map, the permafrost area covers $\sim 1.3 \times 10^4$ km^2, accounting for 30.2% of the watershed."

To be clear, we have also stated at the beginning of the Abstract that "Selin Co, located within permafrost regions surrounded by glaciers, has exhibited the greatest increase in water storage among all the lakes on the Tibetan Plateau over the last 50 years. Most of the increased lake water volume has been attributed to increased precipitation and the accelerated melting of glacier ice, but these processes are still not sufficient to achieve the water balance with the expansion of Selin Co. Ground ice meltwater released by thawing permafrost due to continuous climate warming over the past several decades was regarded as another source of lake expansion."

Thank you for the suggestion. In the revised manuscript, we have added the statements of permafrost map and ground ice as follows.

"(Zou et al., 2017) mapped the permafrost distribution on the Qinghai-Tibet Plateau (QTP) based on freezing and thawing indices from Moderate Resolution Imaging Spectroradiometer (MODIS) land surface temperatures and validated their map using various ground-based datasets; according to this permafrost map, the permafrost area covers $\sim 1.3 \times 10^4$ km^2, accounting for 30.2% of the watershed. Continuous permafrost and seasonally frozen ground exist, with the former being widespread mainly in the northern part of the watershed (Zou et al., 2017). (Zhao and Sheng, 2019) estimated the ground ice storage on the QTP based on the ice content distribution characteristics from 164 drill core records deeper than 15 m, the above permafrost distribution map, a map of the Quaternary sedimentary types, and a permafrost thickness map; based on their map, the ground ice volume in the watershed reaches 132.3 km^3 (Zhao and Sheng, 2019), approximately five times the glacier ice volume in the Selin Co watershed." The 164 drill core records includes along the Qinghai-Tibet engineering corridor, Zhuonai Lake, Altun, West Kunlun Mountains, Gaize, and Wenquan areas), which constructs WE, NS profiles over the Qinghai-Tibet Plateau, and provides the properties of ground ice spatial distribution. The sedimentary type map provides the basic information of soil type.

To be clear, the statement has been rephrased to "we assumed that the amount of surface settlement would release the same amount of ground ice caused by compressing the thawing ice-rich permafrost layer."

Figure 1: enlarge text, numbers, reference point (a cross should be better). Add S-1footprints in a larger area.
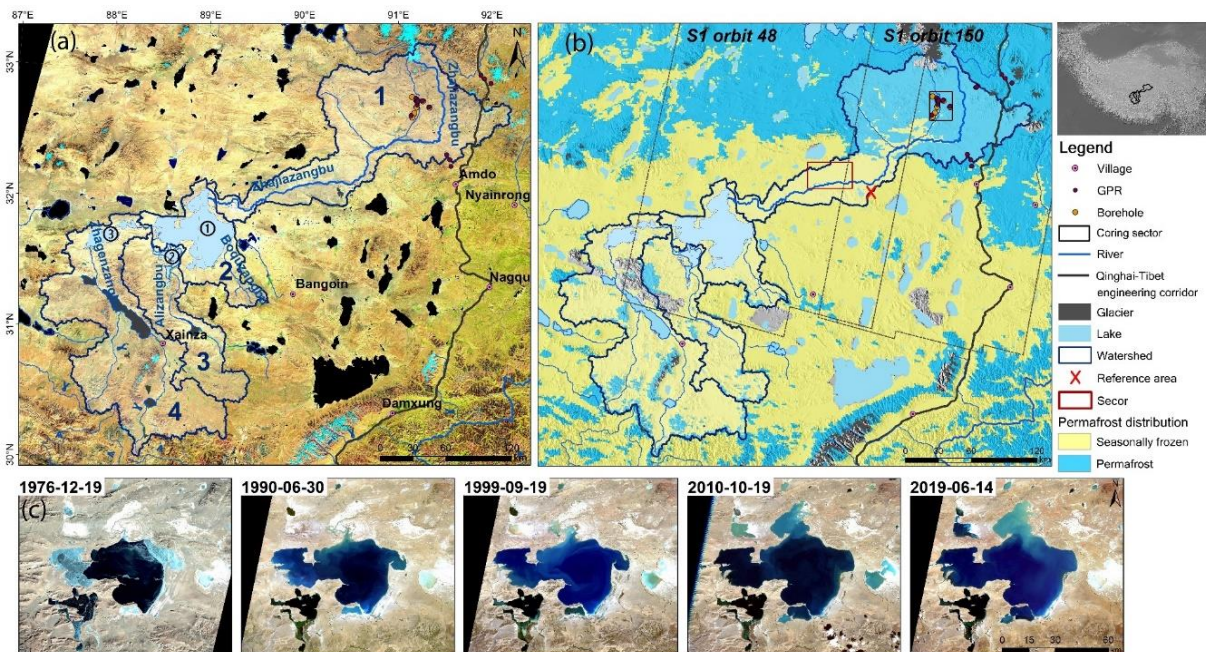Figure 1 has been modified as follows.

Figure 1 Study area. The base map in Fig. 1(a) is a Landsat 8 image acquired in October 2020 (red: SWIR1, green: NIR, blue: red). The base map in Fig. 1(b) is a permafrost map (Zou et al., 2017); the hillshade is calculated using a 1-arcsec SRTM DEM with the Sentinel-1 incidence angle and azimuth angle. The grey dashed lines delineate two tracks of Sentinel-1 used in this study. The red cross marks the position of our InSAR reference point. The locations of the GPR surveys and boreholes are shown with dots. Fig. 1(c) shows the lake areas from 1976 to 2019 on Landsat optical images.

Table 4 : give date in YYYYMMDD format
The dates in the manuscript have been corrected to the YYYYMMDD format.

line 222: " Every SAR image was coregistered…acquisitions". It is not clear. I guess what is meant is that all interferometric pair processing was done independently from each other (without a stack processing that would result in a stack of co-registered image). It is a bit misleading, so may be rewrite this paragraph starting with explaining that each ifg processing was done independently from each other.
Thank you very much for pointing out this misleading expression. There is stack processing during InSAR processing. To be clear, the sentence has been rewritten as "All the SLC images were coregistered to the stack reference of 20180807 acquisition for orbit 150 and 20180801 acquisition for orbit 48. After generating a coregistered stack of SLC images, interferograms were generated by each SAR image with its two sequential acquisitions."

line 238: weighting by the inverse of phase variance: variance in space? over whatarea ? whole interferogram ?

Thank you for the comment. To be clear, the sentence has been rephrased as "During the inversion, interferograms were weighted by the inverse of the phase variance of the whole interferogram (Zhang et al., 2019).."

The weight matrix takes the form:

$$\mathbf{W} = \text{diag} \left\{ 1/\sigma^2_{\Delta\varphi^1}, \dots, 1/\sigma^2_{\Delta\varphi^M} \right\}$$

where $\sigma^2_{\Delta\varphi^j}$ is the phase variance of the j_{th} interferogram calculated through the integration of the phase probability distribution function (PDF).

Like minimum cost flow unwrapping method which provides the global optimal result, the weight used here also evaluates the interferogram in global.

line 239: Please cite the other studies that are referenced here

The studies have been cited in the revised manuscript as follows "Different from some studies conducted in permafrost environments that presupposed deformation models to help solve the phase time series (Li et al., 2015; Chen et al., 2018), we did not preset any deformation and instead obtained the raw phase time series by minimizing the phase residual."

line 271: mosaicking is performed after projection on vertical, so delete here.

Thank you for the comment. During processing, we mosaicked the LOS seasonal amplitude and trend rate and the incidence angle of two orbits as well. The deformations exhibited throughout the manuscript are in the LOS direction. To be clear, we have modified the sentence in the revised manuscript that "For each orbit, we extracted the LOS periodic (seasonal) amplitude and long-term deformation rate pixel by pixel from the deformation time series and then mosaiced the results from the two orbits together. The spatial grids of the incidence angles from the two orbits were mosaiced as well.".

line 274 : "Thus, the observed…direction": delete

This sentence has been removed.

line 275: add "assuming no horizontal displacement"

Thank you. It has been rephrased to "For flat terrain, deformation is caused mainly by freeze–thaw cycles within the permafrost layer and occurs predominantly in the vertical direction. Hence, assuming no horizontal displacement, the observed deformation in the line of the sight (LOS) direction was converted into the vertical direction."

line 288: "long-term…elevation": replace with cumulated settlement

Thank you for the suggestion. It has been corrected.

line 294 /299: if a threshold on velocity, it must be in velocity unit (2.5 mm/yr), so separate thresholds on amplitude and on velocity

Thank you for the suggestion. We've stated these two thresholds separately as follows "masking off areas with the LOS direction periodic (seasonal) amplitudes ≤1.5 mm or long-term velocities ≤2.5 mm/a"

line 391: " This sensitivity…SLC04": drop, repetition.

Thank you. Corrected.

line 394: "surface permafrost" : unclear

The surface permafrost in the original manuscript means we don't consider the situation that the permafrost table is in a very deep place (a few tens of meters). That case is very rare. Thus, it has been replaced with "permafrost" in the revised manuscript to avoid unnecessary misunderstanding.

line 397: SLC03 is repeated twice

Thank you. The second "SLC03" has been deleted.

Fig8: suggestion to put text or symbol or graph of found ice in cores on each panel tofacilitate the reading.

Thank you for the suggestion. We have replotted Fig. 5 and integrated the information on ground ice, and deformation properties (originally listed in Table 7 in the previous manuscript).
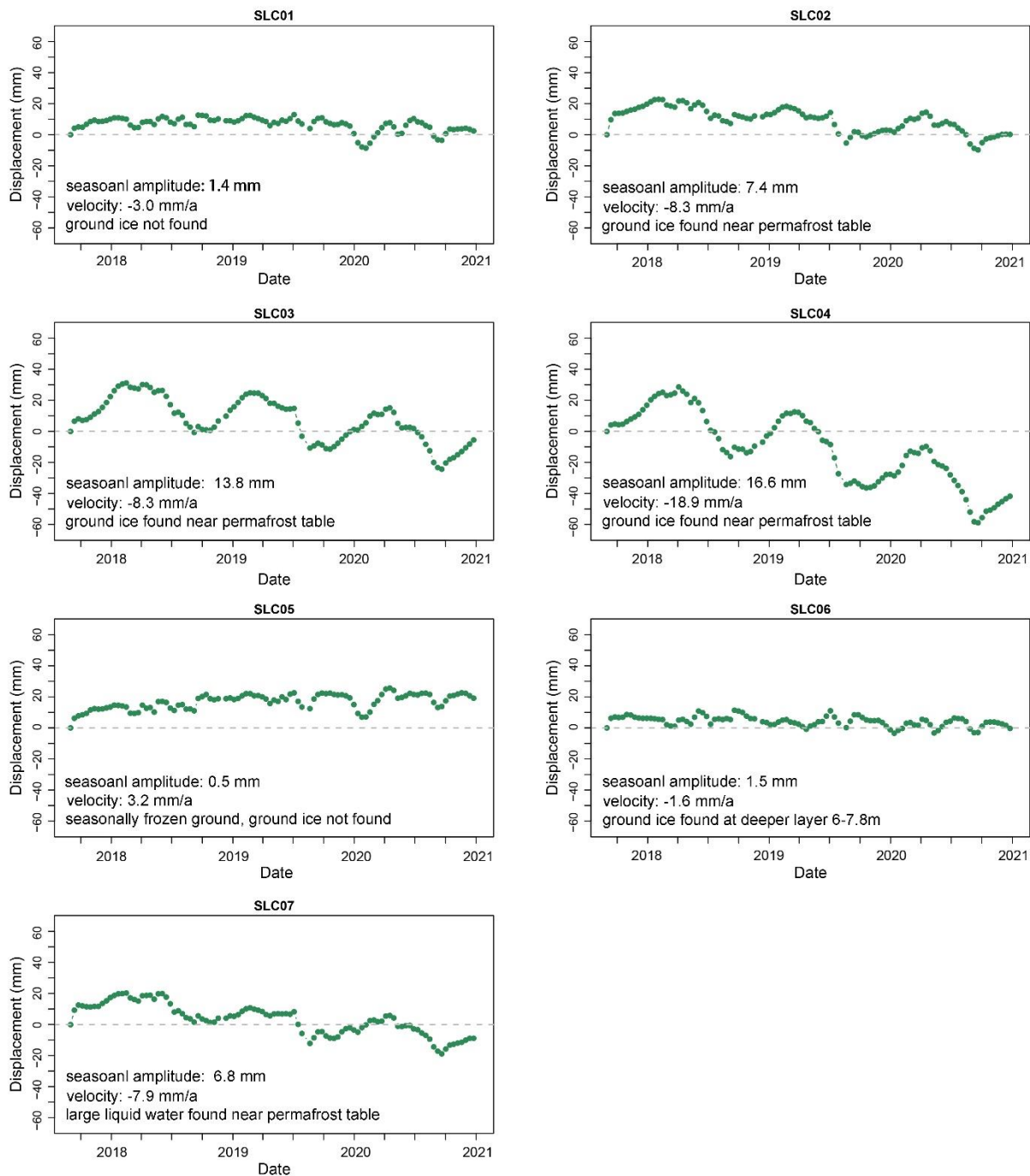
Figure 5 LOS deformation time series at the seven borehole sites. Positive values represent uplift and negative values represent subsidence relative to the first scene of the S1 datasets.

References

Berardino, P., Fornaro, G., Lanari, R., and Sansosti, E.: A new algorithm for surface deformation monitoring based on small baseline differential SAR interferograms, Geoscience and Remote Sensing, IEEE Transactions on, 40, 2375-2383, 2002.

Chen, C. W. and Zebker, H. A.: Phase unwrapping for large SAR interferograms: Statistical segmentation and generalized network models, IEEE Transactions on Geoscience and Remote Sensing, 40, 1709-1719, 2002.

Chen, J., Liu, L., Zhang, T., Cao, B., and Lin, H.: Using persistent scatterer interferometry to map and quantify permafrost thaw subsidence: A case study of Eboling Mountain on the Qinghai-Tibet Plateau, Journal of Geophysical Research: Earth Surface, 123, 2663-2676, 2018.

Cheng, G.: The mechanism of repeated-segregation for the formation of thick layered ground ice, Cold Regions Science and Technology, 8, 57-66, 1983.

Daout, S., Dini, B., Haeberli, W., Doin, M.-P., and Parsons, B.: Ice loss in the Northeastern Tibetan Plateau permafrost as seen by 16 yr of ESA SAR missions, Earth and Planetary Science Letters, 545, 116404, 2020.

French, H. M.: The periglacial environment, John Wiley & Sons2017.

Li, Z., Zhao, R., Hu, J., Wen, L., Feng, G., Zhang, Z., and Wang, Q.: InSAR analysis of surface deformation over permafrost to estimate active layer thickness based on one-dimensional heat transfer model of soils, Scientific reports, 5, 2015.

Pepe, A. and Lanari, R.: On the extension of the minimum cost flow algorithm for phase unwrapping of multitemporal differential SAR interferograms, IEEE Transactions on Geoscience and remote sensing, 44, 2374-2383, 2006.

Zhang, Y., Fattahi, H., and Amelung, F.: Small baseline InSAR time series analysis: Unwrapping error correction and noise reduction, Computers & Geosciences, 133, 104331, 2019.

Zhang, Y., Xie, C., Wu, T., Zhao, L., Wu, J., Wu, X., Li, R., Hu, G., Liu, G., and Wang, W.: New permafrost is forming on the exposed bottom of Zonag Lake on the Qinghai-Tibet Plateau, Science of The Total Environment, 152879, 2022.

Zhao, L. and Sheng, Y.: Permafrost and environment changes on the QinghaiTibetan Plateau (in Chinese), Science Press, Beijing, China2019.

Zou, D., Zhao, L., Yu, S., Chen, J., Hu, G., Wu, T., Wu, J., Xie, C., Wu, X., and Pang, Q.: A new map of permafrost distribution on the Tibetan Plateau, The Cryosphere, 11, 2527, 2017.